

Landscape of somatic mutations in 560 breast cancer whole-genome sequences

Serena Nik-Zainal^{1,2}, Helen Davies¹, Johan Staaf³, Manasa Ramakrishna¹, Dominik Glodzik¹, Xueqing Zou¹, Inigo Martincorena¹, Ludmil B. Alexandrov^{1,4,5}, Sancha Martin¹, David C. Wedge¹, Peter Van Loo^{1,6}, Young Seok Ju¹, Marcel Smid⁷, Arie B. Brinkman⁸, Sandro Morganello⁹, Miriam R. Aure^{10,11}, Ole Christian Lingjærde^{11,12}, Anita Langerød^{10,11}, Markus Ringnér³, Sung-Min Ahn¹³, Sandrine Boyault¹⁴, Jane E. Brock¹⁵, Annegien Broeks¹⁶, Adam Butler¹, Christine Desmedt¹⁷, Luc Dirix¹⁸, Serge Dronov¹, Aquila Fatima¹⁹, John A. Foekens⁷, Moritz Gerstung¹, Gerrit K. J. Hooijer²⁰, Se Jin Jang²¹, David R. Jones¹, Hyung-Yong Kim²², Tari A. King²³, Savitri Krishnamurthy²⁴, Hee Jin Lee²¹, Jeong-Yeon Lee²⁵, Yilong Li¹, Stuart McLaren¹, Andrew Menzies¹, Ville Mustonen¹, Sarah O'Meara¹, Iris Pauporté²⁶, Xavier Pivot²⁷, Colin A. Purdie²⁸, Keiran Raine¹, Kamna Ramakrishnan¹, F. Germán Rodríguez-González⁷, Gilles Romieu²⁹, Anieta M. Sieuwerts⁷, Peter T. Simpson³⁰, Rebecca Shepherd¹, Lucy Stebbings¹, Olafur A. Stefansson³¹, Jon Teague¹, Stefania Tommasi³², Isabelle Treilleux³³, Gert G. Van den Eynden^{18,34}, Peter Vermeulen^{18,34}, Anne Vincent-Salomon³⁵, Lucy Yates¹, Carlos Caldas³⁶, Laura van't Veer¹⁶, Andrew Tutt^{37,38}, Stian Knappskog^{39,40}, Benita Kiat Tee Tan^{41,42}, Jos Jonkers¹⁶, Åke Borg³, Naoto T. Ueno²⁴, Christos Sotiriou¹⁷, Alain Viari^{43,44}, P. Andrew Futreal^{1,45}, Peter J. Campbell¹, Paul N. Span⁴⁶, Steven Van Laere¹⁸, Sunil R. Lakhani^{30,47}, Jorunn E. Eyfjord³¹, Alastair M. Thompson^{28,48}, Ewan Birney⁹, Hendrik G. Stunnenberg⁸, Marc J. van de Vijver²⁰, John W. M. Martens⁷, Anne-Lise Børresen-Dale^{10,11}, Andrea L. Richardson^{15,19}, Gu Kong²², Gilles Thomas⁴⁴ & Michael R. Stratton¹

We analysed whole-genome sequences of 560 breast cancers to advance understanding of the driver mutations conferring clonal advantage and the mutational processes generating somatic mutations. We found that 93 protein-coding cancer genes carried probable driver mutations. Some non-coding regions exhibited high mutation frequencies, but most have distinctive structural features probably causing elevated mutation rates and do not contain driver mutations. Mutational signature analysis was extended to genome rearrangements and revealed twelve base substitution and six rearrangement signatures. Three rearrangement signatures, characterized by tandem duplications or deletions, appear associated with defective homologous-recombination-based DNA repair: one with deficient BRCA1 function, another with deficient BRCA1 or BRCA2 function, the cause of the third is unknown. This analysis of all classes of somatic mutation across exons, introns and intergenic regions highlights the repertoire of cancer genes and mutational processes operating, and progresses towards a comprehensive account of the somatic genetic basis of breast cancer.

The mutational theory of cancer proposes that changes in DNA sequence, termed 'driver' mutations, confer proliferative advantage on a cell, leading to outgrowth of a neoplastic clone¹. Some driver mutations are inherited in the germline, but most arise in

somatic cells during the lifetime of the cancer patient, together with many 'passenger' mutations not implicated in cancer development¹. Multiple mutational processes, including endogenous and exogenous mutagen exposures, aberrant DNA editing, replication errors

¹Wellcome Trust Sanger Institute, Hinxton, Cambridge CB10 1SA, UK. ²East Anglian Medical Genetics Service, Cambridge University Hospitals NHS Foundation Trust, Cambridge CB2 9NB, UK. ³Division of Oncology and Pathology, Department of Clinical Sciences Lund, Lund University, Lund SE-223 81, Sweden. ⁴Theoretical Biology and Biophysics (T-6), Los Alamos National Laboratory, Los Alamos, NM 87545, New Mexico, USA. ⁵Center for Nonlinear Studies, Los Alamos National Laboratory, Los Alamos, New Mexico 87545, USA. ⁶Department of Human Genetics, University of Leuven, B-3000 Leuven, Belgium. ⁷Department of Medical Oncology, Erasmus MC Cancer Institute and Cancer Genomics Netherlands, Erasmus University Medical Center, Rotterdam 3015CN, The Netherlands. ⁸Radboud University, Department of Molecular Biology, Faculty of Science, 6525GA Nijmegen, The Netherlands. ⁹European Molecular Biology Laboratory, European Bioinformatics Institute, Wellcome Trust Genome Campus, Hinxton, Cambridge CB10 1SD, UK. ¹⁰Department of Cancer Genetics, Institute for Cancer Research, Oslo University Hospital, The Norwegian Radium Hospital, Oslo 0310, Norway. ¹¹K. G. Jebsen Centre for Breast Cancer Research, Institute for Clinical Medicine, University of Oslo, Oslo 0310, Norway. ¹²Department of Computer Science, University of Oslo, Oslo, Norway. ¹³Gachon Institute of Genome Medicine and Science, Gachon University Gil Medical Center, Incheon, South Korea. ¹⁴Translational Research Lab, Centre Léon Bérard, 28, rue Laënnec, 69373 Lyon Cedex 08, France. ¹⁵Department of Pathology, Brigham and Women's Hospital, Boston, Massachusetts 02115, USA. ¹⁶The Netherlands Cancer Institute, 1066 CX Amsterdam, The Netherlands. ¹⁷Breast Cancer Translational Research Laboratory, Université Libre de Bruxelles, Institut Jules Bordet, Bd de Waterloo 121, B-1000 Brussels, Belgium. ¹⁸Translational Cancer Research Unit, Center for Oncological Research, Faculty of Medicine and Health Sciences, University of Antwerp, Antwerp, Belgium. ¹⁹Dana-Farber Cancer Institute, Boston, Massachusetts 02215, USA. ²⁰Department of Pathology, Academic Medical Center, Meibergdreef 9, 1105 AZ Amsterdam, The Netherlands. ²¹Department of Pathology, Asan Medical Center, College of Medicine, Ulsan University, Ulsan, South Korea. ²²Department of Pathology, College of Medicine, Hanyang University, Seoul 133-791, South Korea. ²³Memorial Sloan Kettering Cancer Center, 1275 York Avenue, New York, New York 10065, USA. ²⁴Morgan Welch Inflammatory Breast Cancer Research Program and Clinic, The University of Texas MD Anderson Cancer Center, 1515 Holcombe Boulevard, Houston, Texas 77030, USA. ²⁵Institute for Bioengineering and Biopharmaceutical Research (IBBR), Hanyang University, Seoul, South Korea. ²⁶Institut National du Cancer, Research Division, Clinical Research Department, 52 avenue Morizet, 92513 Boulogne-Billancourt, France. ²⁷University Hospital of Minjoo, INSERM UMR 1098, Bd Fleming, Besançon 25000, France. ²⁸Pathology Department, Ninewells Hospital and Medical School, Dundee DD1 9SY, UK. ²⁹Oncologie Sénologie, ICM Institut Régional du Cancer, Montpellier, France. ³⁰The University of Queensland, UQ Centre for Clinical Research and School of Medicine, Brisbane, Queensland 4029, Australia. ³¹Cancer Research Laboratory, Faculty of Medicine, University of Iceland, 101 Reykjavik, Iceland. ³²IRCCS Istituto Tumori "Giovanni Paolo II", Bari, Italy. ³³Department of Pathology, Centre Léon Bérard, 28 rue Laënnec, 69373 Lyon Cedex 08, France. ³⁴Department of Pathology, GZA Hospitals Sint-Augustinus, Antwerp, Belgium. ³⁵Institut Curie, Paris Sciences Lettres University, Department of Pathology and INSERM U934, 26 rue d'Ulm, 75248 Paris Cedex 05, France. ³⁶Cancer Research UK Cambridge Institute, University of Cambridge, Li Ka Shing Centre, Robinson Way, Cambridge CB2 0RE, UK. ³⁷Breast Cancer Now Research Unit, King's College London, London SE1 9RT, UK. ³⁸Breast Cancer Now Toby Robins Research Center, Institute of Cancer Research, London SW3 6JB, UK. ³⁹Department of Clinical Science, University of Bergen, 5020 Bergen, Norway. ⁴⁰Department of Oncology, Haukeland University Hospital, 5021 Bergen, Norway. ⁴¹National Cancer Centre Singapore, 11 Hospital Drive, 169610, Singapore. ⁴²Singapore General Hospital, Outram Road, 169608, Singapore. ⁴³Equipe Erable, INRIA Grenoble-Rhône-Alpes, 655, Avenue de l'Europe, 38330 Montbonnot-Saint Martin, France. ⁴⁴Synergie Lyon Cancer, Centre Léon Bérard, 28 rue Laënnec, Lyon Cedex 08, France. ⁴⁵Department of Genomic Medicine, UT MD Anderson Cancer Center, Houston, Texas 77230, USA. ⁴⁶Department of Radiation Oncology, Department of Laboratory Medicine, Radboud University Medical Center, Nijmegen 6525GA, The Netherlands. ⁴⁷Pathology Queensland, The Royal Brisbane and Women's Hospital, Brisbane, Queensland 4029, Australia. ⁴⁸Department of Breast Surgical Oncology, University of Texas MD Anderson Cancer Center, 1400 Pressler Street, Houston, Texas 77030, USA.

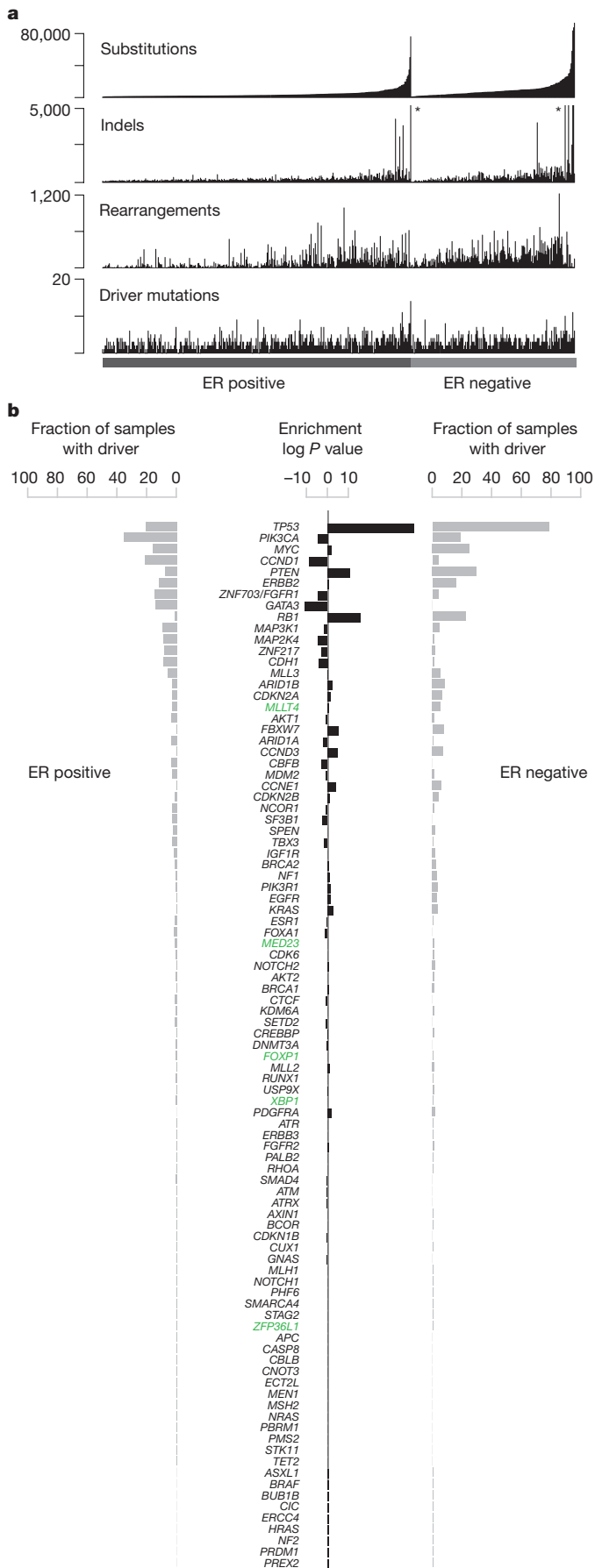


Figure 1 | Cohort and catalogue of somatic mutations in 560 breast cancers. **a**, Catalogue of base substitutions, insertions/deletions, rearrangements and driver mutations in 560 breast cancers (sorted by total substitution burden). Indel axis limited to 5,000(*). **b**, Complete list of curated driver genes sorted by frequency (descending). Fraction of ER-positive (left, total 366) and ER-negative (right, total 194) samples carrying a mutation in the relevant driver gene presented in grey. $\log_{10} P$ value of enrichment of each driver gene towards the ER-positive or ER-negative cohort is provided in black. Highlighted in green are genes for which there is new or further evidence supporting these as novel breast cancer genes.

and defective DNA maintenance, are responsible for generating these mutations¹⁻³.

Over the past five decades, several waves of technology have advanced the characterization of mutations in cancer genomes. Karyotype analysis revealed rearranged chromosomes and copy number alterations. Subsequently, loss of heterozygosity analysis, hybridization of cancer-derived DNA to microarrays and other approaches provided higher resolution insights into copy number changes⁴⁻⁸. Recently, DNA sequencing has enabled systematic characterization of the full repertoire of mutation types including base substitutions, small insertions/deletions, rearrangements and copy number changes⁹⁻¹³, yielding substantial insights into the mutated cancer genes and mutational processes operative in human cancer.

As for many cancer classes, most currently available breast cancer genome sequences target protein-coding exons^{8,11-15}. Consequently, there has been limited consideration of mutations in untranslated, intronic and intergenic regions, leaving central questions pertaining to the molecular pathogenesis of the disease unresolved. First, the role of activating driver rearrangements¹⁶⁻¹⁸ forming chimaeric (fusion) genes/proteins or relocating genes adjacent to new regulatory regions as observed in haematological and other malignancies¹⁹. Second, the role of driver substitutions and indels in non-coding regions of the genome^{20,21}. Common inherited variants conferring susceptibility to human disease are generally in non-coding regulatory regions and the possibility that similar mechanisms operate somatically in cancer was highlighted by the discovery of somatic driver substitutions in the *TERT* gene promoter^{22,23}. Third, which mutational processes generate the somatic mutations found in breast cancer^{2,24}. Addressing this question has been constrained because exome sequences do not inform on genome rearrangements and capture relatively few base substitution mutations, thus limiting statistical power to extract the mutational signatures imprinted on the genome by these processes^{24,25}.

Here we analyse whole-genome sequences of 560 cases in order to address these and other questions and to pave the way to a comprehensive understanding of the origins and consequences of somatic mutations in breast cancer.

Cancer genes and driver mutations

The whole genomes of 560 breast cancers and non-neoplastic tissue from each individual (556 female and 4 male) were sequenced (Supplementary Fig. 1, Supplementary Table 1). We detected 3,479,652 somatic base substitutions, 371,993 small indels and 77,695 rearrangements, with substantial variation in the number of each between individual samples (Fig. 1a, Supplementary Table 3). Transcriptome sequence, microRNA expression, array-based copy number and DNA methylation data were obtained from subsets of cases.

To identify new cancer genes, we combined somatic substitutions and indels in protein-coding exons with data from other series^{12-15,26}, constituting a total of 1,332 breast cancers, and searched for mutation clustering in each gene beyond that expected by chance. Five cancer genes were found for which evidence was previously absent or equivocal (*MED23*, *FOXP1*, *MLLT4*, *XBPI*, *ZFP36L1*), or for which the mutations indicate the gene acts in breast cancer in a recessive rather than in a dominant fashion, as previously reported in other cancer types (see Supplementary Methods section 7.4 for detailed descriptions). From published reports on all cancer types (<http://cancer.sanger.ac.uk/census>),

we then compiled a list of 727 human cancer genes (Supplementary Table 12). On the basis of driver mutations found previously, we defined conservative rules for somatic driver base substitutions and indel mutations in each gene and sought mutations conforming to these rules in the 560 breast cancers. We identified 916 probable driver mutations of these classes (Fig. 1b, Supplementary Table 14, Extended Data Fig. 1).

To explore the role of genomic rearrangements as driver mutations^{16,18,19,27}, we sought predicted in-frame fusion genes that might create activated, dominant cancer genes. We identified 1,278 unique and 39 infrequently recurrent in-frame gene fusions (Supplementary Table 15). Many of the latter, however, were in regions of high rearrangement density, including amplicons²⁸ and fragile sites, and their recurrence is probably attributable to chance²⁷. Furthermore, transcriptome sequences from 260 cancers did not show expression of these fusions and generally confirmed the rarity of recurrent in-frame fusion genes. By contrast, recurrent rearrangements interrupting the gene footprints of *CDKN2A*, *RBI*, *MAP3K1*, *PTEN*, *MAP2K4*, *ARID1B*, *FBXW7*, *MLLT4* and *TP53* were found beyond the numbers expected from local background rearrangement rates, indicating that they contribute to the driver mutation burden of recessive cancer genes. Several other recurrently rearranged genomic regions were observed, including dominantly acting cancer genes *ETV6* and *ESR1* (without consistent elevation in expression levels), L1 retrotransposition sites²⁹ and fragile sites. The significance of these recurrently rearranged regions remains unclear (Extended Data Fig. 2).

Incorporation of recurrent copy number changes, including homozygous deletions and amplifications, generated a total of 1,628 likely driver mutations in 93 cancer genes (Fig. 1b). At least one driver was identifiable in 95% of cancers. The 10 most frequently mutated genes were *TP53*, *PIK3CA*, *MYC*, *CCND1*, *PTEN*, *ERBB2*, *ZNF703/FGFR1* locus, *GATA3*, *RBI* and *MAP3K1* (Fig. 1b, Extended Data Fig. 1), and these accounted for 62% of drivers.

Recurrent somatic mutations in non-coding regions

To investigate non-coding somatic driver substitutions and indels, we searched for non-coding genomic regions with more mutations than expected by chance (Fig. 2a, Supplementary Table 16, Extended Data Fig. 3).

The promoter of *PLEKHS1* exhibited recurrent mutations at two genomic positions³⁰ (Fig. 2a) TTTTGCAAT TGAACA ATTGCAAAA (as previously reported³⁰). The two mutated bases, within a 6 base pair (bp) core motif, are flanked, on either side by 9 base pairs of palindromic sequence forming inverted repeats³¹. Most cancers with these mutations showed many base substitutions of mutational signatures 2 and 13 that have been attributed to activity of APOBEC DNA-editing proteins that target the TCN sequence motif. One of the mutated bases is a cytosine in a TCA sequence context (shown above as the reverse complement, TGA) at which predominantly C>T substitutions were found. The other is a cytosine in ACA context, which showed both C>T and C>G mutations.

The TGAACA core sequence was mutated at the same two positions at multiple locations elsewhere in the genome (Supplementary Table 16c) where the TGAACA core was also flanked by palindromes albeit of different sequences and lengths (Supplementary Table 16c). These mutations were also usually found in cancers with many signature 2 and 13 mutations (Fig. 2a). TGAACA core sequences with longer flanking palindromes generally exhibited a higher mutation rate, and TGAACA sequences flanked by 9 bp palindromes exhibited an ~265-fold higher mutation rate than sequences without them (Fig. 2b, Supplementary Table 16d). However, additional factors must influence the mutation rate because it varied markedly between TGAACA core sequences with different palindromes of the same length (Fig. 2c). Some TGAACA-inverted repeat sites were in regulatory regions but others were intronic or intergenic without functional annotation (examples in Supplementary Table 16c) or exonic. The propensity for mutation recurrence at specific positions in a distinctive sequence motif in cancers with numerous mutations of particular signatures renders it plausible that these are hypermutable hotspots^{32–34}, perhaps through formation of DNA hairpin structures³⁵, which are single-stranded at their tips enabling attack by APOBEC enzymes, rather than driver mutations.

Two recurrently mutated sites were also observed in the promoter of *TBCID12* (TBC1 domain family, member 12) (q value 4.5×10^{-2}) (Fig. 2a). The mutations were characteristic of signatures 2 and 13 and enriched in cancers with many signature 2 and 13 mutations (Fig. 2a). The mutations were within the *TBCID12* Kozak consensus sequence

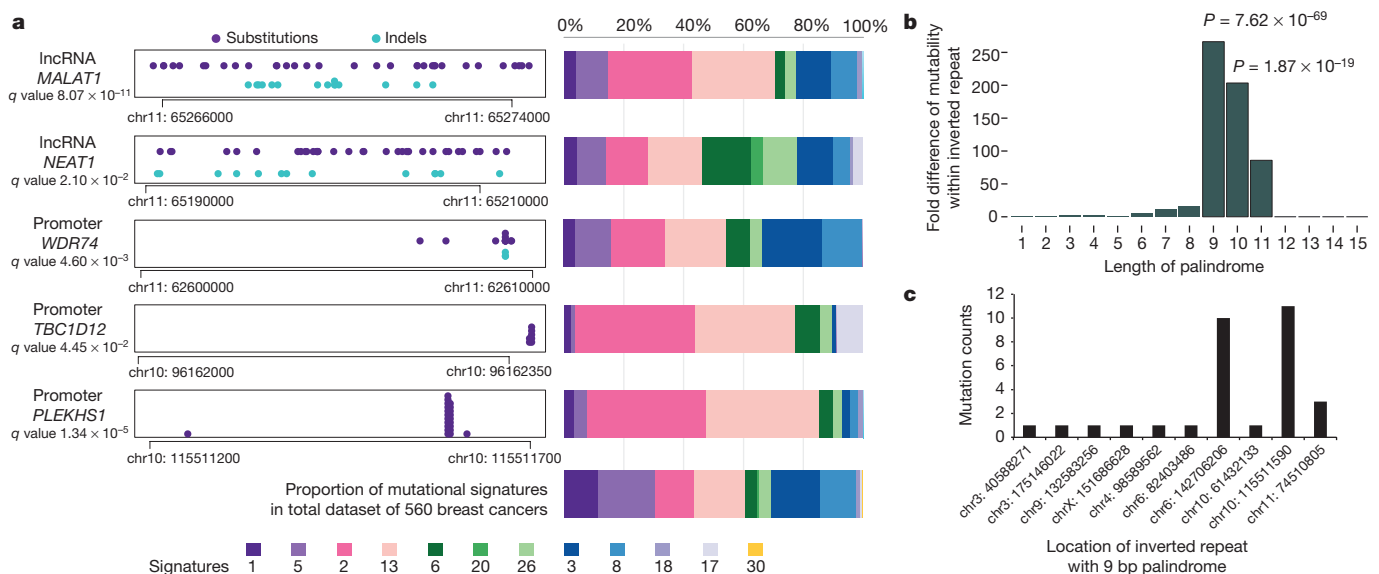


Figure 2 | Non-coding analyses of breast cancer genomes.

a, Distributions of substitution (purple dots) and indel (blue dots) mutations within the footprint of five regulatory regions identified as being more significantly mutated than expected is provided on the left. The proportion of base substitution mutation signatures associated with corresponding samples carrying mutations in each of these non-coding

regions, is displayed on the right. **b**, Mutability of TGAACA/TGTTCA motifs within inverted repeats of varying flanking palindromic sequence length compared to motifs not within an inverted repeat. **c**, Variation in mutability between loci of TGAACA/TGTTCA inverted repeats with 9 bp palindromes.

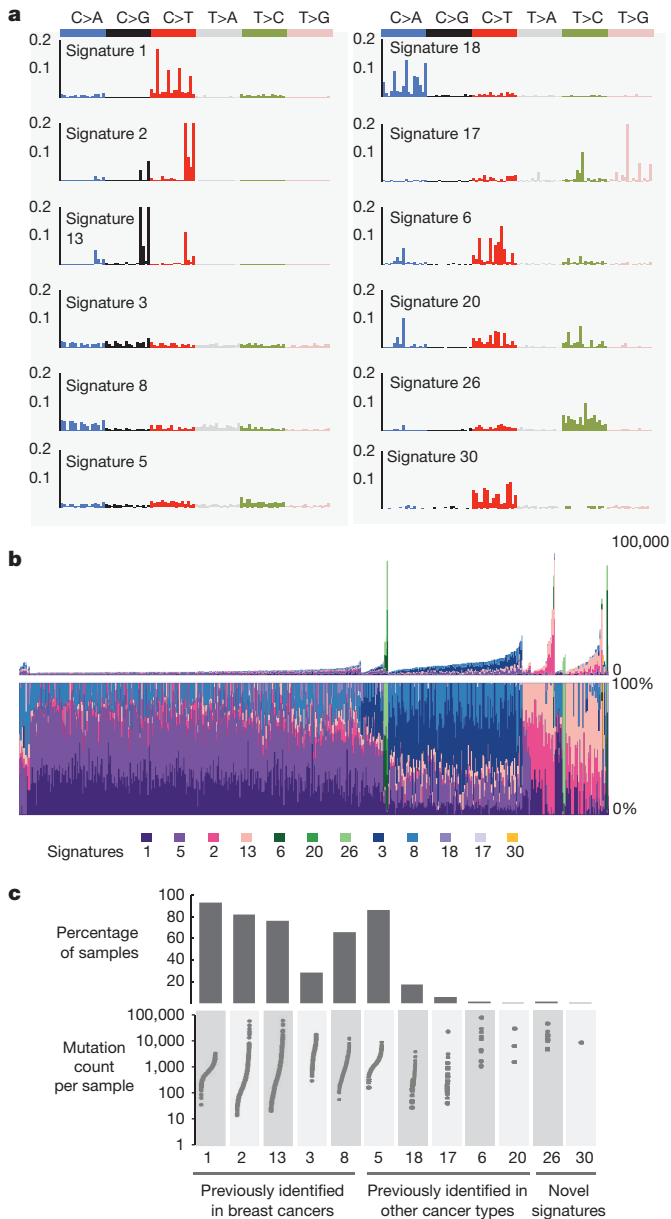


Figure 3 | Extraction and contributions of base substitution signatures in 560 breast cancers. **a**, Twelve mutation signatures extracted using non-negative matrix factorization. Each signature is ordered by mutation class (C>A/G>T, C>G/G>C, C>T/G>A, T>A/A>T, T>C/A>G, T>G/A>C), taking immediate flanking sequence into account. For each class, mutations are ordered by 5' base (A, C, G, T) first before 3' base (A, C, G, T). **b**, The spectrum of base substitution signatures within 560 breast cancers. Mutation signatures are ordered (and coloured) according to broad biological groups: signatures 1 and 5 are correlated with age of diagnosis; signatures 2 and 13 are putatively APOBEC-related; signatures 6, 20 and 26 are associated with mismatch-repair deficiency; signatures 3 and 8 are associated with homologous-recombination deficiency; signatures 18, 17 and 30 have unknown aetiology. For ease of reading, this arrangement is adopted for the rest of the manuscript. Samples are ordered according to hierarchical clustering performed on mutation signatures. Top, absolute numbers of mutations of each signature in each sample. Bottom, proportion of each signature in each sample. **c**, Distribution of mutation counts for each signature in relevant breast cancer samples. Percentage of samples carrying each signature provided above each signature.

(CCCCAGATGGTGGG)), shifting it away from the consensus³⁶. The association with particular mutational signatures suggests that these may also be in a region of hypermutability rather than drivers.

The *WDR74* promoter showed base substitutions and indels (q value 4.6×10^{-3}) forming a cluster of overlapping mutations²⁰ (Fig. 2a). Coding sequence driver mutations in *WDR74* have not been reported. No differences were observed in *WDR74* transcript levels between cancers with *WDR74* promoter mutations compared to those without. Nevertheless, the pattern of this non-coding mutation cluster, with overlapping and different mutation types, is more compatible with the possibility of the mutations being drivers.

Two long non-coding RNAs, *MALAT1* (q value 8.7×10^{-11} , as previously reported¹²) and *NEAT1* (q value 2.1×10^{-2}) were enriched with mutations. Transcript levels were not significantly different between mutated and non-mutated samples. Whether these mutations are drivers or result from local hypermutability is unclear.

Mutational signatures

Mutational processes generating somatic mutations imprint particular patterns of mutations on cancer genomes, termed signatures^{2,24,37}. Applying a mathematical approach²⁵ to extract mutational signatures previously revealed five base-substitution signatures in breast cancer: signatures 1, 2, 3, 8 and 13 (refs 2, 24). Using this method for the 560 cases revealed twelve signatures, including those previously observed and a further seven, of which five have formerly been detected in other cancer types (signatures 5, 6, 17, 18 and 20) and two are new (signatures 26 and 30) (Fig. 3a, b, 4a, Supplementary Table 21a–c, Supplementary Methods section 15). Two indel signatures were also found^{2,24}.

Signatures of rearrangement mutational processes have not previously been formally investigated. To enable this we adopted a rearrangement classification incorporating 32 subclasses. In many cancer genomes, large numbers of rearrangements are regionally clustered, for example in zones of gene amplification. Therefore, we first classified rearrangements into those inside and outside clusters, further subclassified them into deletions, inversions and tandem duplications, and then according to the size of the rearranged segment. The final category in both groups was interchromosomal translocations.

Application of the mathematical framework used for base substitution signatures^{2,24,25} extracted six rearrangement signatures (Fig. 4b, Supplementary Table 21). Unsupervised hierarchical clustering on the basis of the proportion of rearrangements attributed to each signature in each breast cancer yielded seven major subgroups exhibiting distinct associations with other genomic, histological or gene expression features (Fig. 5, Extended Data Figs 4–6).

Rearrangement signature 1 (9% of all rearrangements) and rearrangement signature 3 (18% rearrangements) were characterized predominantly by tandem duplications (Fig. 4b). Tandem duplications associated with rearrangement signature 1 were mostly >100 kb (Fig. 4b), and those with rearrangement signature 3 were <10 kb (Fig. 4b, Extended Data Fig. 7). More than 95% of rearrangement signature 3 tandem duplications were concentrated in 15% of cancers (cluster D, Fig. 5), many with several hundred rearrangements of this type. Almost all cancers (91%) with *BRCA1* mutations or promoter hypermethylation were in this group, which was enriched for basal-like, triple negative cancers and copy number classification of a high homologous recombination deficiency (HRD) index^{38–40}. Thus, inactivation of *BRCA1*, but not *BRCA2*, may be responsible for the rearrangement signature 3 small tandem duplication mutator phenotype.

More than 35% of rearrangement signature 1 tandem duplications were found in just 8.5% of the breast cancers and some cases had hundreds of these (cluster F, Fig. 5). The cause of this large tandem duplication mutator phenotype (Fig. 4b) is unknown. Cancers exhibiting it are frequently TP53-mutated, relatively late diagnosis, triple-negative breast cancers, showing enrichment for base substitution signature 3 and a high HRD index (Fig. 5), but do not have *BRCA1/2* mutations or *BRCA1* promoter hypermethylation.

Rearrangement signature 1 and 3 tandem duplications (Extended Data Fig. 7) were generally evenly distributed over the genome. However,

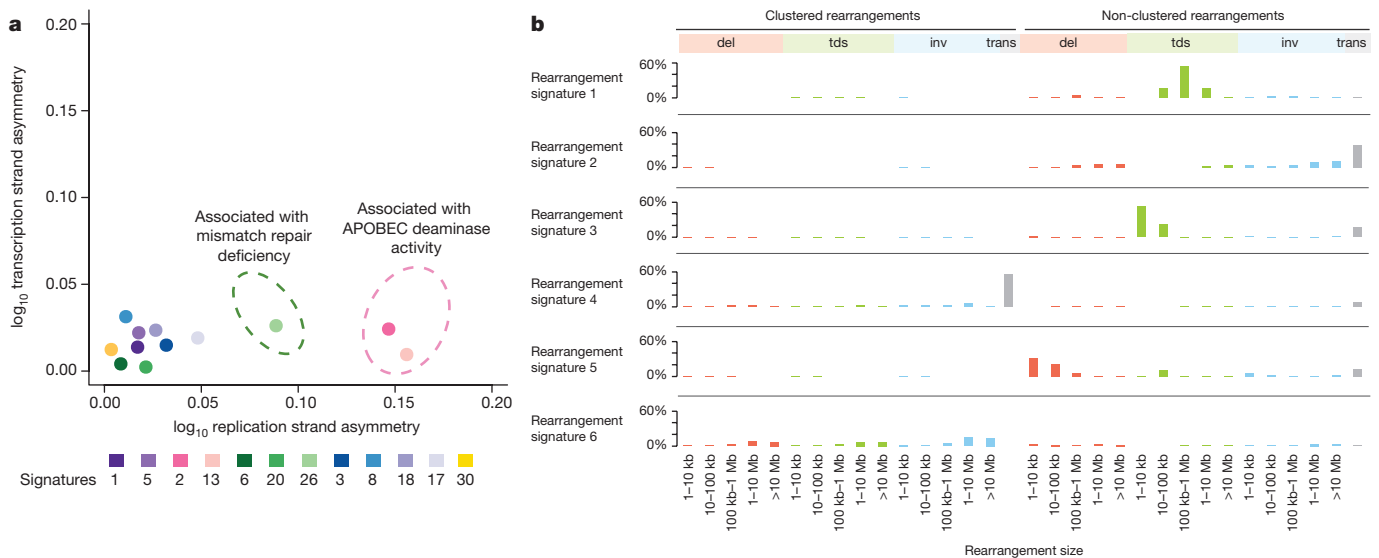


Figure 4 | Additional characteristics of base substitution signatures and novel rearrangement signatures in 560 breast cancers. a, Contrasting transcriptional strand asymmetry and replication strand asymmetry between twelve base substitution signatures. **b**, Six rearrangement

there were nine locations at which recurrence of tandem duplications was found across the breast cancers and which often showed multiple, nested tandem duplications in individual cases (Extended Data Fig. 8). These may be mutational hotspots specific for these tandem duplication mutational processes, although we cannot exclude the possibility that they represent driver events.

Rearrangement signature 5 (accounting for 14% rearrangements) was characterized by deletions <100 kb. It was strongly associated with the presence of *BRCA1* mutations or promoter hypermethylation (cluster D, Fig. 5), *BRCA2* mutations (cluster G, Fig. 5) and with rearrangement signature 1 large tandem duplications (cluster F, Fig. 5).

Rearrangement signature 2 (accounting for 22% rearrangements) was characterized by non-clustered deletions (>100 kb), inversions and interchromosomal translocations, was present in most cancers but was particularly enriched in oestrogen receptor (ER)-positive cancers with quiet copy number profiles (cluster E, GISTIC (genomic identification of significant targets in cancer) cluster 3; Fig. 5). Rearrangement signature 4 (accounting for 18% of rearrangements) was characterized by clustered interchromosomal translocations, whereas rearrangement signature 6 (19% of rearrangements) had clustered inversions and deletions (clusters A, B, C; Fig. 5).

Short segments (1–5 bp) of overlapping microhomology characteristic of alternative methods of end-joining repair were found at most rearrangements^{2,14}. Rearrangement signatures 2, 4 and 6 were characterized by a peak at 1 bp of microhomology, whereas rearrangement signatures 1, 3 and 5, associated with homologous recombination DNA repair deficiency, exhibited a peak at 2 bp (Extended Data Fig. 9). Thus, different end-joining mechanisms may operate with different rearrangement processes. A proportion of breast cancers showed rearrangement signature 5 deletions with longer (>10 bp) microhomologies involving sequences from short-interspersed nuclear elements, most commonly AluS (63%) and AluY (15%) family repeats (Extended Data Fig. 9). Long segments (more than 10 bp) of non-templated sequence were particularly enriched amongst clustered rearrangements.

Localized hypermutation: kataegis

Focal base-substitution hypermutation, termed kataegis, is generally characterized by substitutions with characteristic features of signatures 2 and 13 (refs 2, 24). Kataegis was observed in 49% breast cancers, with 4% exhibiting 10 or more foci (Supplementary Table 21c). Kataegis colocalizes with clustered rearrangements characteristic of rearrangement

signatures extracted using non-negative matrix factorization. Probability of rearrangement element on y axis. Rearrangement size on x axis. del, deletion; tds, tandem duplication; inv, inversion; trans, translocation.

signatures 4 and 6 (Fig. 4b). Cancers with tandem duplications or deletions of rearrangement signatures 1, 3 and 5 did not usually demonstrate kataegis. However, there must be additional determinants of kataegis as only 2% of rearrangements are associated with it. A rare (14 out of 1,557 foci, 0.9%) alternative form of kataegis, colocalizing with rearrangements but with a base-substitution pattern characterized by T>G and T>C mutations, predominantly at NTT and NTA sequences (where N can be any base A, T, C or G), was also observed (Extended Data Fig. 10). This pattern of base substitutions most closely matches signature 9 (Extended Data Fig. 10; <http://cancer.sanger.ac.uk/cosmic/signatures>), previously observed in B lymphocyte neoplasms and attributed to polymerase eta activity⁴¹.

Mutational signatures exhibit distinct DNA replication strand biases

The distributions of mutations attributable to each of the 20 mutational signatures (12 base substitution, 2 indel and 6 rearrangement) were explored⁴² with respect to DNA replication strand. We found an asymmetric distribution of mutations between leading and lagging replication strands for many, but not all signatures⁴² (Fig. 4a). Notably, signatures 2 and 13, owing to APOBEC deamination, showed marked lagging-strand replication bias (Fig. 4a) suggesting that lagging-strand replication provides single-stranded DNA for APOBEC deamination. Of the three signatures associated with mismatch-repair deficiency (signatures 6, 20 and 26), only signature 26 exhibited replicative-strand bias, highlighting how different signatures arising from defects of the same pathway can exhibit distinct relationships with replication.

Mutational signatures associated with *BRCA1* and *BRCA2* mutations

Of the 560 breast cancers, 90 had germline (60) or somatic (14) inactivating mutations in *BRCA1* (35) or *BRCA2* (39) or showed methylation of the *BRCA1* promoter (16). Loss of the wild-type chromosome 17 or 13 was observed in 80 out of 90 cases. The latter exhibited many base substitution mutations of signature 3, accompanied by deletions of >3 bp with microhomology at rearrangement break-points, and signature 8 together with CC>AA double nucleotide substitutions. Cases in which the wild-type chromosome 17 or 13 was retained did not show these signatures. Thus signature 3 and, to a lesser extent, signature 8 are associated with absence of *BRCA1* and *BRCA2* functions.

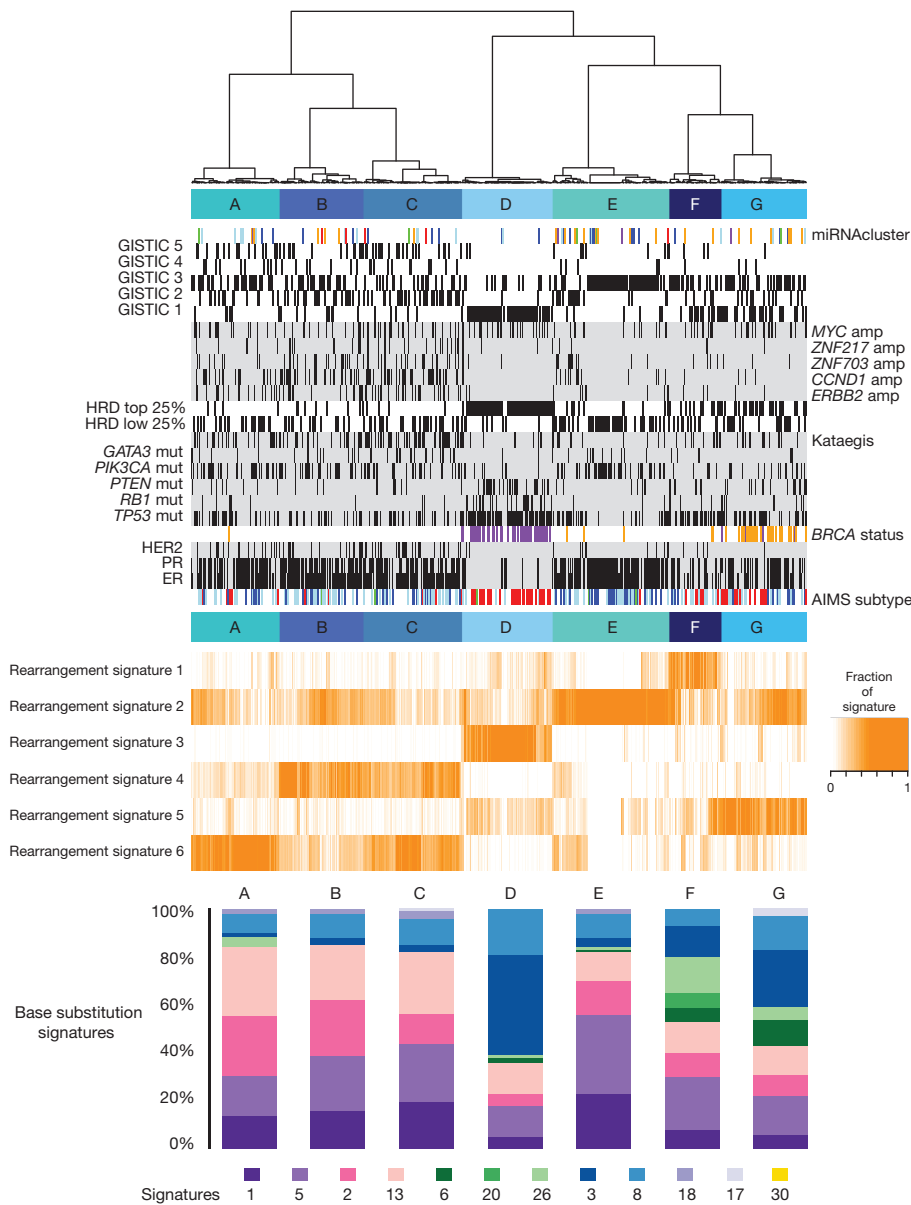


Figure 5 | Integrative analysis of rearrangement signatures. Heatmap of rearrangement signatures following unsupervised hierarchical clustering based on proportions of rearrangement signatures in each cancer. Seven cluster groups (A–G) noted and relationships with expression (AIMS) subtype (basal, red; luminal B, light blue; luminal A, dark blue), immunohistopathology status (ER, progesterone receptor (PR), HER2 status; black, positive), abrogation of *BRCA1* (purple) and *BRCA2* (orange) (whether germline, somatic or through promoter hypermethylation), presence of 3 or more foci of kataegis (black, positive), HRD index (top 25% or lowest 25%; black, positive), GISTIC cluster group (black, positive) and driver mutations in cancer genes. miRNA cluster groups: 0, red; 1, purple; 2, blue; 3, light blue; 4, green; 5, orange. Contribution of base-substitution signatures in these seven cluster groups is provided in the bottom panel.

Cancers with inactivating *BRCA1* or *BRCA2* mutations usually carry many genomic rearrangements. Cancers with *BRCA1*, but not *BRCA2*, mutations exhibit large numbers of rearrangement signature 3 small tandem duplications. Cancers with *BRCA1* or *BRCA2* mutations show substantial numbers of rearrangement signature 5 deletions. No other rearrangement signatures were associated with *BRCA1*- or *BRCA2*-null cases (clusters D and G, Fig. 5). Some breast cancers without identifiable *BRCA1/2* mutations or *BRCA1* promoter methylation showed these features and segregated with *BRCA1/2*-null cancers in hierarchical clustering analysis (Fig. 5). In such cases, the *BRCA1/2* mutations may have been missed or other mutated or promoter methylated genes may be exerting similar effects (see <http://cancer.sanger.ac.uk/cosmic/sample/genomes> for examples of whole-genome profiles of typical *BRCA1*-null, (for example, PD6413a, PD7215a) and *BRCA2*-null tumours (for example, PD4952a, PD4955a)).

A further subset of cancers (cluster F, Fig. 5) show similarities in mutational pattern to *BRCA1/2*-null cancers, with many rearrangement signature 5 deletions and enrichment for base substitution signatures 3 and 8. However, these do not segregate together with *BRCA1/2*-null cases in hierarchical clustering analysis, have rearrangement signature 1 large tandem duplications and do not show *BRCA1/2* mutations. Somatic and germline mutations in genes associated with the DNA

double-strand break repair pathway including *ATM*, *ATR*, *PALB2*, *RAD51C*, *RAD50*, *TP53*, *CHEK2* and *BRIP1*, were sought in these cancers. We did not observe any clear-cut relationships between mutations in these genes and these mutational patterns.

Cancers with *BRCA1/2* mutations are particularly responsive to cisplatin and PARP inhibitors^{43–45}. Combinations of base substitution, indel and rearrangement mutational signatures may be better biomarkers of defective homologous-recombination-based DNA double-strand break repair and responsiveness to these drugs⁴⁶ than *BRCA1/2* mutations or promoter methylation alone and thus may constitute the basis of future diagnostics.

Conclusions

A comprehensive perspective on the somatic genetics of breast cancer is drawing closer (see <http://cancer.sanger.ac.uk/cosmic/sample/genomes> for individual patient genome profile, and Methods for orientation). At least 12 base substitution mutational signatures and 6 rearrangement signatures contribute to the somatic mutations found, and 93 mutated cancer genes (31 dominant, 60 recessive, 2 uncertain) are implicated in genesis of the disease. However, dominantly acting activated fusion genes and non-coding driver mutations appear rare. Additional infrequently mutated cancer genes probably exist.

However, the genes harbouring the substantial majority of driver mutations are now known.

Nevertheless, important questions remain to be addressed. Recurrent mutational events including whole-chromosome copy number changes and unexplained regions with recurrent rearrangements could harbour additional cancer genes. Identifying non-coding drivers is challenging and requires further investigation. Although almost all breast cancers have at least one identifiable driver mutation, the number with only a single identified driver is perhaps surprising. The roles of viruses or other microbes have not been exhaustively examined. Thus, further exploration and analysis of whole-genome sequences from breast cancer patients will be required to complete our understanding of the somatic mutational basis of the disease.

Online Content Methods, along with any additional Extended Data display items and Source Data, are available in the online version of the paper; references unique to these sections appear only in the online paper.

Received 29 June 2015; accepted 17 March 2016.

Published online 2 May 2016.

- Stratton, M. R., Campbell, P. J. & Futreal, P. A. The cancer genome. *Nature* **458**, 719–724 (2009).
- Nik-Zainal, S. *et al.* Mutational processes molding the genomes of 21 breast cancers. *Cell* **149**, 979–993 (2012).
- Nik-Zainal, S. *et al.* The life history of 21 breast cancers. *Cell* **149**, 994–1007 (2012).
- Hicks, J. *et al.* Novel patterns of genome rearrangement and their association with survival in breast cancer. *Genome Res.* **16**, 1465–1479 (2006).
- Bergamaschi, A. *et al.* Extracellular matrix signature identifies breast cancer subgroups with different clinical outcome. *J. Pathol.* **214**, 357–367 (2008).
- Ching, H. C., Naidu, R., Seong, M. K., Har, Y. C. & Taib, N. A. Integrated analysis of copy number and loss of heterozygosity in primary breast carcinomas using high-density SNP array. *Int. J. Oncol.* **39**, 621–633 (2011).
- Fang, M. *et al.* Genomic differences between estrogen receptor (ER)-positive and ER-negative human breast carcinoma identified by single nucleotide polymorphism array comparative genome hybridization analysis. *Cancer* **117**, 2024–2034 (2011).
- Curtis, C. *et al.* The genomic and transcriptomic architecture of 2,000 breast tumours reveals novel subgroups. *Nature* **486**, 346–352 (2012).
- Pleasance, E. D. *et al.* A comprehensive catalogue of somatic mutations from a human cancer genome. *Nature* **463**, 191–196 (2010).
- Pleasance, E. D. *et al.* A small-cell lung cancer genome with complex signatures of tobacco exposure. *Nature* **463**, 184–190 (2010).
- Banerji, S. *et al.* Sequence analysis of mutations and translocations across breast cancer subtypes. *Nature* **486**, 405–409 (2012).
- Ellis, M. J. *et al.* Whole-genome analysis informs breast cancer response to aromatase inhibition. *Nature* **486**, 353–360 (2012).
- Shah, S. P. *et al.* The clonal and mutational evolution spectrum of primary triple-negative breast cancers. *Nature* **486**, 395–399 (2012).
- Stephens, P. J. *et al.* The landscape of cancer genes and mutational processes in breast cancer. *Nature* **486**, 400–404 (2012).
- The Cancer Genome Atlas Network Comprehensive molecular portraits of human breast tumours. *Nature* **490**, 61–70 (2012).
- Wu, Y. M. *et al.* Identification of targetable FGFR gene fusions in diverse cancers. *Cancer Discovery* **3**, 636–647 (2013).
- Giacomini, C. P. *et al.* Breakpoint analysis of transcriptional and genomic profiles uncovers novel gene fusions spanning multiple human cancer types. *PLoS Genet.* **9**, e1003464 (2013).
- Robinson, D. R. *et al.* Functionally recurrent rearrangements of the MAST kinase and Notch gene families in breast cancer. *Nature Med.* **17**, 1646–1651 (2011).
- Karlsson, J. *et al.* Activation of human telomerase reverse transcriptase through gene fusion in clear cell sarcoma of the kidney. *Cancer Lett.* **357**, 498–501 (2015).
- Khurana, E. *et al.* Integrative annotation of variants from 1092 humans: application to cancer genomics. *Science* **342**, 1235587 (2013).
- West, J. A. *et al.* The long noncoding RNAs NEAT1 and MALAT1 bind active chromatin sites. *Mol. Cell* **55**, 791–802 (2014).
- Huang, F. W. *et al.* Highly recurrent *TERT* promoter mutations in human melanoma. *Science* **339**, 957–959 (2013).
- Vinagre, J. *et al.* Frequency of *TERT* promoter mutations in human cancers. *Nature Commun.* **4**, 2185 (2013).
- Alexandrov, L. B. *et al.* Signatures of mutational processes in human cancer. *Nature* **500**, 415–421 (2013).
- Alexandrov, L. B., Nik-Zainal, S., Wedge, D. C., Campbell, P. J. & Stratton, M. R. Deciphering signatures of mutational processes operative in human cancer. *Cell Rep.* **3**, 246–259 (2013).
- Lawrence, M. S. *et al.* Discovery and saturation analysis of cancer genes across 21 tumour types. *Nature* **505**, 495–501 (2014).
- Natrajan, R. *et al.* Characterization of the genomic features and expressed fusion genes in micropapillary carcinomas of the breast. *J. Pathol.* **232**, 553–565 (2014).
- Kalyana-Sundaram, S. *et al.* Gene fusions associated with recurrent amplicons represent a class of passenger aberrations in breast cancer. *Neoplasia* **14**, 702–708 (2012).
- Tubio, J. M. Somatic structural variation and cancer. *Brief. Funct. Genomics* **14**, 339–351 (2015).
- Weinhold, N., Jacobsen, A., Schultz, N., Sander, C. & Lee, W. Genome-wide analysis of noncoding regulatory mutations in cancer. *Nature Genet.* **46**, 1160–1165 (2014).
- Ussery, D. W., Binnewies, T. T., Gouveia-Oliveira, R., Jarmer, H. & Hallin, P. F. Genome update: DNA repeats in bacterial genomes. *Microbiology* **150**, 3519–3521 (2004).
- Lu, S. *et al.* Short inverted repeats are hotspots for genetic instability: relevance to cancer genomes. *Cell Rep.* **10**, 1674–1680 (2015).
- Voineagu, I., Narayanan, V., Lobachev, K. S. & Mirkin, S. M. Replication stalling at unstable inverted repeats: interplay between DNA hairpins and fork stabilizing proteins. *Proc. Natl Acad. Sci. USA* **105**, 9936–9941 (2008).
- Wojcik, E. A. *et al.* Direct and inverted repeats elicit genetic instability by both exploiting and eluding DNA double-strand break repair systems in mycobacteria. *PLoS ONE* **7**, e51064 (2012).
- Pearson, C. E., Zorbas, H., Price, G. B. & Zannis-Hadjopoulos, M. Inverted repeats, stem-loops, and cruciforms: significance for initiation of DNA replication. *J. Cell. Biochem.* **63**, 1–22 (1996).
- Kozak, M. Interpreting cDNA sequences: some insights from studies on translation. *Mamm. Genome* **7**, 563–574 (1996).
- Helleday, T., Eshtad, S. & Nik-Zainal, S. Mechanisms underlying mutational signatures in human cancers. *Nature Rev. Genet.* **15**, 585–598 (2014).
- Birkbak, N. J. *et al.* Telomeric allelic imbalance indicates defective DNA repair and sensitivity to DNA-damaging agents. *Cancer Disc.* **2**, 366–375 (2012).
- Abkevich, V. *et al.* Patterns of genomic loss of heterozygosity predict homologous recombination repair defects in epithelial ovarian cancer. *Br. J. Cancer* **107**, 1776–1782 (2012).
- Popova, T. *et al.* Ploidy and large-scale genomic instability consistently identify basal-like breast carcinomas with *BRCA1/2* inactivation. *Cancer Res.* **72**, 5454–5462 (2012).
- Puente, X. S. *et al.* Whole-genome sequencing identifies recurrent mutations in chronic lymphocytic leukaemia. *Nature* **475**, 101–105 (2011).
- Morganella, S. A. *et al.* The topography of mutational processes in breast cancer genomes. *Nature Commun.* <http://dx.doi.org/10.1038/ncomms11383> (2016).
- Fong, P. C. *et al.* Inhibition of poly(ADP-ribose) polymerase in tumors from BRCA mutation carriers. *N. Engl. J. Med.* **361**, 123–134 (2009).
- Forster, M. D. *et al.* Treatment with olaparib in a patient with PTEN-deficient endometrioid endometrial cancer. *Nature Rev. Clin. Oncol.* **8**, 302–306 (2011).
- Turner, N., Tutt, A. & Ashworth, A. Targeting the DNA repair defect of BRCA tumours. *Curr. Opin. Pharmacol.* **5**, 388–393 (2005).
- Waddell, N. *et al.* Whole genomes redefine the mutational landscape of pancreatic cancer. *Nature* **518**, 495–501 (2015).

Supplementary Information is available in the online version of the paper.

Acknowledgements This work has been funded through the ICGC Breast Cancer Working group by the Breast Cancer Somatic Genetics Study (BASIS), a European research project funded by the European Community's Seventh Framework Programme (FP7/2010-2014) under the grant agreement number 242006; the Triple Negative project funded by the Wellcome Trust (grant reference 077012/Z/05/Z) and the HER2+ project funded by Institut National du Cancer (INCa) in France (grant numbers 226-2009, 02-2011, 41-2012, 144-2008, 06-2012). The ICGC Asian Breast Cancer Project was funded through a grant of the Korean Health Technology R&D Project, Ministry of Health and Welfare, Republic of Korea (A11218-SC01). Personally funded by grants above: F.G.R.-G., S.M., K.R., S.M. were funded by BASIS. Recruitment was performed under the auspices of the ICGC breast cancer projects run by the UK, France and Korea. For contributions towards instruments, specimens and collections: Tayside Tissue Bank (funded by CRUK, University of Dundee, Chief Scientist Office & Breast Cancer Campaign), Asan Bio-Resource Center of the Korea Biobank Network, Seoul, South Korea, OSBREAC consortium, The Icelandic Centre for Research (RANNIS), The Swedish Cancer Society and the Swedish Research Council, and Fondation Jean Dausset-Centre d'Etudes du polymorphisme humain, Icelandic Cancer Registry, The Brisbane Breast Bank (The University of Queensland, The Royal Brisbane and Women's Hospital and QIMR Berghofer), Breast Cancer Tissue and Data Bank at KCL and NIHR Biomedical Research Centre at Guy's and St Thomas's Hospitals. Breakthrough Breast Cancer and Cancer Research UK Experimental Cancer Medicine Centre at KCL. For pathology review: The Mouse Genome Project and Department of Pathology, Cambridge University Hospitals NHS Foundation Trust for microscopes. A. Richardson, A. Ehinger, A. Vincent-Salomon, C. Van Deurzen, C. Purdie, D. Larsimont, D. Giri, D. Grabau, E. Provenzano, G. MacGrogan, G. Van den Eynden, I. Treilleux, J. E. Brock, J. Jacquemier, J. Reis-Filho, L. Arnould, L. Jones, M. van de Vijver, Ø. Garred, R. Salgado, S. Pinder, S. R. Lakhani, T. Sauer, V. Barbashina. Illumina UK Ltd for input on optimization of sequencing throughout this project. Wellcome Trust Sanger Institute Sequencing Core Facility, Core IT Facility and Cancer Genome Project Core IT

team and Cancer Genome Project Core Laboratory team for general support. Personal funding: S.N.-Z. is a Wellcome Beit Fellow and personally funded by a Wellcome Trust Intermediate Fellowship (WT100183MA). L.B.A. is supported through a J. Robert Oppenheimer Fellowship at Los Alamos National Laboratory. A.L.R. is partially supported by the Dana-Farber/Harvard Cancer Center SPORC in Breast Cancer (NIH/NCI 5 P50 CA168504-02). D.G. was supported by the EU-FP7-SUPPRESSTEM project. A.S. was supported by Cancer Genomics Netherlands through a grant from the Netherlands Organisation of Scientific research (NWO). M.S. was supported by the EU-FP7-DDR response project. C.S. and C.D. are supported by a grant from the Breast Cancer Research Foundation. E.B. was funded by EMBL. C.S. is funded by FNRS (Fonds National de la Recherche Scientifique). S.J.J. is supported by Leading Foreign Research Institute Recruitment Program through the National Research Foundation of Republic Korea (NRF 2011-0030105). G.K. is supported by National Research Foundation of Korea (NRF) grants funded by the Korean government (NRF 2015R1A2A1A10052578). J.F. received funding from an ERC Advanced grant (no. 322737). For general contribution and administrative support: Fondation Synergie Lyon Cancer in France. J. G. Jonasson, Department of Pathology, University Hospital & Faculty of Medicine, University of Iceland. K. Ferguson, Tissue Bank Manager, Brisbane Breast Bank and The Breast Unit, The Royal Brisbane and Women's Hospital, Brisbane, Australia. The Oslo Breast Cancer Consortium of Norway (OSBREAC). Angelo Paradiso, IRCCS Istituto Tumori "Giovanni Paolo II", Bari Italy. A. Vines for administratively supporting to identifying the samples, organizing the bank, and sending out the samples. M. Schlooz-Vries, J. Tol, H. van Laarhoven, F. Sweep, P. Bult in Nijmegen for contributions in Nijmegen. This research used resources provided by the Los Alamos National Laboratory Institutional Computing Program, which is supported by the US Department of Energy National Nuclear Security Administration under contract no. DE-AC52-06NA25396. Research performed at Los Alamos National Laboratory was carried out under the auspices of the National Nuclear Security Administration of the United States Department of

Energy. N. Miller (in memoriam) for her contribution in setting up the clinical database. Finally, we would like to acknowledge all members of the ICGC Breast Cancer Working Group and ICGC Asian Breast Cancer Project.

Author Contributions S.N.-Z., M.R.S. designed the study, analysed data and wrote the manuscript. H.D., J.S., M. Ramakrishna, D.G., X.Z. performed curation of data and contributed towards genomic and copy number analyses. M.S., A.B.B., M.R.A., O.C.L., A.L., M. Ringner, contributed towards curation and analysis of non-genomic data (transcriptomic, miRNA, methylation). I.M., L.B.A., D.C.W., P.V.L., S. Morganello, Y.S.J., contributed towards specialist analyses. G.T., G.K., A.L.R., A-L.B.-D., J.W.M.M., M.J.v.d.V., H.G.S., E.B., A. Borg., A.V., P.A.F., P.J.C., designed the study, drove the consortium and provided samples. S.Martin was the project coordinator. S.McL., S.O.M., K.R., contributed operationally. S.-M.A., S.B., J.E.B., A.Brooks., C.D., L.D., A.F., J.A.F., G.K.J.H., S.J.J., H.-Y.K., T.A.K., S.K., H.J.L., J.-Y.L., I.P., X.P., C.A.P., F.G.R.-G., G.R., A.M.S., P.T.S., O.A.S., S.T., I.T., G.G.V.d.E., P.V., A.V.-S., L.Y., C.C., L.v.V., A.T., S.K., B.K.T.T., J.J., N.t.U., C.S., P.N.S., S.V.L., S.R.L., J.E.E., A.M.T. contributed pathology assessment and/or samples. A. Butler, S.D., M.G., D.R.J., Y.L., A.M., V.M., K.R., R.S., L.S., J.T. contributed IT processing and management expertise. All authors discussed the results and commented on the manuscript.

Author Information Raw data have been submitted to the European-Genome Phenome Archive under the overarching accession number EGAS00001001178 (please see Supplementary Notes for breakdown by data type). Somatic variants have been deposited at the International Cancer Genome Consortium Data Portal (<https://dcc.icgc.org/>). Reprints and permissions information is available at www.nature.com/reprints. The authors declare no competing financial interests. Readers are welcome to comment on the online version of the paper. Correspondence and requests for materials should be addressed to G.K. (gkong@hanyang.ac.kr), S.N.-Z. (snz@sanger.ac.uk), M.S. (mrs@sanger.ac.uk) or A.V. (Alain.Viari@inria.fr).

METHODS

Data reporting. No statistical methods were used to predetermine sample size. The experiments were not randomized and the investigators were not blinded to allocation during experiments and outcome assessment.

Sample selection. DNA was extracted from 560 breast cancers and normal tissue (peripheral blood lymphocytes, adjacent normal breast tissue or skin) and total RNA extracted from 268 of the same individuals. Samples were subjected to pathology review and only samples assessed as being composed of >70% tumour cells, were accepted for inclusion in the study (Supplementary Table 1).

Massively parallel sequencing and alignment. Short insert 500 bp genomic libraries and 350 bp poly-A-selected transcriptomic libraries were constructed, flowcells prepared and sequencing clusters generated according to Illumina library protocols⁴⁷. We performed 108 base/100 base (genomic), or 75 base (transcriptomic) paired-end sequencing on Illumina GAIIx, HiSeq 2000 or HiSeq 2500 genome analysers, in accordance with the Illumina Genome Analyzer operating manual. The average sequence coverage was 40.4-fold for tumour samples and 30.2-fold for normal samples (Supplementary Table 2).

Short insert paired-end reads were aligned to the reference human genome (GRCh37) using Burrows-Wheeler Aligner, BWA (v0.5.9)⁴⁸. RNA sequencing data was aligned to the human reference genome (GRCh37) using TopHat (v1.3.3) (<http://ccb.jhu.edu/software/tophat/index.shtml>).

Processing of genomic data. CaVEMan (Cancer Variants Through Expectation Maximization: <http://cancerit.github.io/CaVEMan/>) was used for calling somatic substitutions.

Indels in the tumour and normal genomes were called using a modified Pindel version 2.0. (<http://cancerit.github.io/cgpPindel/>) on the NCBI37 genome build⁴⁹.

Structural variants were discovered using a bespoke algorithm, BRASS (BReakpoint AnalySiS) (<https://github.com/cancerit/BRASS>) through discordantly mapping paired-end reads. Next, discordantly mapping read pairs that were likely to span breakpoints, as well as a selection of nearby properly paired reads, were grouped for each region of interest. Using the Velvet *de novo* assembler⁵⁰, reads were locally assembled within each of these regions to produce a contiguous consensus sequence of each region. Rearrangements, represented by reads from the rearranged derivative as well as the corresponding non-rearranged allele were instantly recognizable from a particular pattern of five vertices in the de Bruijn graph (a mathematical method used in *de novo* assembly of (short) read sequences) component of Velvet. Exact coordinates and features of junction sequence (for example, microhomology or non-templated sequence) were derived from this, following aligning to the reference genome, as though they were split reads.

See Supplementary Table 3 for summary of somatic variants. Annotation was according to ENSEMBL version 58.

Single nucleotide polymorphism (SNP) array hybridization using the Affymetrix SNP6.0 platform was performed according to Affymetrix protocols. Allele-specific copy number analysis of tumours was performed using ASCAT (v2.1.1), to generate integral allele-specific copy number profiles for the tumour cells⁵¹ (Supplementary Tables 4 and 5). ASCAT was also applied to next-generation sequencing data directly with highly comparable results.

We sampled 12.5% of the breast cancers for validation of substitutions, indels and/or rearrangements in order to make an assessment of the positive predictive value of mutation calling (Supplementary Table 6).

Further details of these processing steps as well as processing of transcriptomic and miRNA data (Supplementary Tables 7 and 8) can be found in Supplementary Methods.

Identification of novel breast cancer genes. To identify recurrently mutated driver genes, a dN/dS method that considers the mutation spectrum, the sequence of each gene, the impact of coding substitutions (synonymous, missense, nonsense, splice site) and the variation of the mutation rate across genes^{52,53} was used for substitutions (Supplementary Table 9). Owing to the lack of a neutral reference for the indel rate in coding sequences, a different approach was required (Supplementary Table 10, Supplementary Methods for details). To detect genes under significant selective pressure by either point mutations or indels, for each gene, the *P* values from the dN/dS analysis of substitutions and from the recurrence analysis of indels were combined using Fisher's method. Multiple testing correction (Benjamini-Hochberg FDR) was performed separately for the more than 600 putative driver genes and for all other genes, stratifying the FDR correction to increase sensitivity (as described in ref. 54). To achieve a low false discovery rate, a conservative *q*-value cutoff of <0.01 was used to determine statistical significance (Supplementary Table 11).

This analysis was applied to the new whole-genome sequences of 560 breast cancers as well as a further 772 breast cancers that have been sequenced previously by other institutions.

See Supplementary Methods for detailed explanations of these methods.

Recurrence in the non-coding regions. *Partitioning the genome into functional regulatory elements/gene features.* To identify non-coding regions with significant recurrence, we used a method similar to the one described for searching for novel indel drivers (see Supplementary Methods for detailed description).

The genome was partitioned according to different sets of regulatory elements/gene features, with a separate analysis performed for each set of elements, including exons ($n = 20,245$ genes), core promoters ($n = 20,245$ genes, where a core promoter is the interval $(-250, +250)$ bp from any transcription start site (TSS) of a coding transcript of the gene, excluding any overlap with coding regions), 5' UTR ($n = 9,576$ genes), 3' UTR ($n = 19,502$ genes), intronic regions flanking exons ($n = 20,212$ genes, represents any intronic sequence within 75 bp from an exon, excluding any base overlapping with any of the above elements), any other sequence within genes ($n = 18,591$ genes, for every protein-coding gene, this contains any region within the start and end of transcripts not included in any of the above categories), non-coding RNAs (ncRNAs) ($n = 10,684$, full length lincRNAs, miRNAs or rRNAs), enhancers⁵⁵ ($n = 194,054$), ultra-conserved regions ($n = 187,057$, a collection of regions under negative selection based on 1,000 genomes data²⁰).

Every element set listed above was analysed separately to allow for different mutation rates across element types and to stratify the FDR correction⁵⁴. Within each set of elements, we used a negative binomial regression approach to learn the underlying variation of the mutation rate across elements. The offset reflects the expected number of mutations in each element assuming uniform mutation rates across them (that is, $E_{\text{subs,element}} = \sum_{j \in \{1,2,\dots,192\}} (r_j S_j t)$, and, $E_{\text{indels,element}} = \mu_{\text{indel}} S_{\text{indel,element}}$) (see Supplementary Methods 7 for a detailed description and definition of all parameters). As covariate here we used the local density of mutations in neighbouring non-coding regions, corrected for sequence composition and trinucleotide mutation rates (that is, the *t* parameter of the dN/dS equations described in section 7.1 of Supplementary Methods). Normalized local rates were pre-calculated for 100 kb non-overlapping bins of the genome and used in all analyses. Other covariates (expression, replication time or Hi-C (genome-wide chromosome conformation capture)) were not used here as they were not found to substantially improve the model once the local mutation rate was used as a covariate. A separate regression analysis was performed for substitutions and indels, to account for the different level of uncertainty in the distribution of substitution and indel rates across elements.

$$\text{model}_{\text{subs}} = \text{glm.nb}(\text{formula} = n_{\text{subs}} \sim \text{offset}(\log(E_{\text{subs}})) + \mu_{\text{local,subs}})$$

$$\text{model}_{\text{indels}} = \text{glm.nb}(\text{formula} = n_{\text{indels}} \sim \text{offset}(\log(E_{\text{indels}})) + \mu_{\text{local,indels}})$$

The observed counts for each element ($n_{\text{subs,element}}$ and $n_{\text{indels,element}}$) are compared to the background distributions using a negative binomial test, with the estimated overdispersion parameters (θ_{subs} and θ_{indels}) estimated by the negative binomial regression, yielding *P* values for substitution and indel recurrence for each element. These *P* values were combined using Fisher's method and corrected for multiple testing using FDR (Supplementary Table 16a).

Partitioning the genome into discrete bins. We performed a genome-wide screening of recurrence in 1 kb non-overlapping bins. We employed the method described in earlier section, using as covariate the local mutation rate calculated from 5 Mb up and downstream from the bin of interest and excluding any low-coverage region from the estimate (Supplementary Table 16b, Extended Data Fig. 3a for example). Significant hits were subjected to manual curation to remove false positives caused by sequencing or mapping artefacts.

Mutational signatures analysis. Mutational signatures analysis was performed following a three-step process: (i) hierarchical *de novo* extraction based on somatic substitutions and their immediate sequence context, (ii) updating the set of consensus signatures using the mutational signatures extracted from breast cancer genomes, and (iii) evaluating the contributions of each of the updated consensus signatures in each of the breast cancer samples. These three steps are discussed in more details in the next sections.

Hierarchical de novo extraction of mutational signatures. The mutational catalogues of the 560 breast cancer whole genome sequences were analysed for mutational signatures using a hierarchical version of the Wellcome Trust Sanger Institute mutational signatures framework²⁵. Briefly, we converted all mutation data into a matrix, *M*, that is made up of 96 features comprising mutations counts for each mutation type (C>A, C>G, C>T, T>A, T>C, and T>G; all substitutions are referred to by the pyrimidine of the mutated Watson-Crick base pair) using each possible 5' (C, A, G, and T) and 3' (C, A, G, and T) context for all samples. After conversion, the previously developed algorithm was applied in a hierarchical manner to the matrix *M* that contains *K* mutation types and *G* samples. The algorithm deciphers the minimal set of mutational signatures that optimally explains the proportion of each mutation type and then estimates the contribution of each signature across the samples. More specifically, the algorithm makes use of a

well-known blind source separation technique, termed non-negative matrix factorization (NNMF). NNMF identifies the matrix of mutational signature, P , and the matrix of the exposures of these signatures, E , by minimizing a Frobenius norm, while maintaining non-negativity:

$$\min_{P \in \mathbb{M}_{R+}^{(K, N)}, E \in \mathbb{M}_{R+}^{(N, G)}} \|M - PE\|_F^2$$

K is the number of mutation types (that is, 96), and \tilde{K} is the number of mutation types after dimensionality reduction. $P \in \mathbb{M}_{R+}^{(K, N)}$ is a matrix of real non-negative numbers of dimension $K \times N$. $E \in \mathbb{M}_{R+}^{(N, G)}$ is a matrix of real non-negative numbers of dimension $N \times G$. The method for deciphering mutational signatures, including evaluation with simulated data and list of limitations, can be found in ref. 25. The framework was applied in a hierarchical manner to increase its ability to find mutational signatures present in few samples as well as mutational signatures exhibiting a low mutational burden. More specifically, after application to the original matrix M containing 560 samples, we evaluated the accuracy of explaining the mutational patterns of each of the 560 breast cancers with the extracted mutational signatures. All samples that were well-explained by the extracted mutational signatures were removed and the framework was applied to the remaining sub-matrix of M . This procedure was repeated until the extraction process did not reveal any new mutational signatures. Overall, the approach extracted 12 unique mutational signatures operative across the 560 breast cancers (Fig. 3, Supplementary Table 21). *Updating the set of consensus mutational signatures.* The 12 hierarchically extracted breast cancer signatures were compared to the census of consensus mutational signatures²⁵. Of the 12 signatures, 11 closely resembled previously identified mutational patterns. The patterns of these 11 signatures, weighted by the numbers of mutations contributed by each signature in the breast cancer data, were used to update the set of consensus mutational signatures as previously performed in ref. 25. One of the 12 extracted signatures is novel and at present, unique for breast cancer. This novel signature is consensus signature 30 (<http://cancer.sanger.ac.uk/cosmic/signatures>).

Evaluating the contributions of consensus mutational signatures in 560 breast cancers. The complete compendium of consensus mutational signatures that was found in breast cancer includes: signatures 1, 2, 3, 5, 6, 8, 13, 17, 18, 20, 26, and 30. We evaluated the presence of all of these signatures in the 560 breast cancer genomes by re-introducing them into each sample. More specifically, the updated set of consensus mutational signatures was used to minimize the constrained linear function for each sample:

$$\min_{e_i \geq 0} \|\mathbf{m} - \sum_{i=1}^N (\mathbf{p}_i e_i)\|_F^2$$

Here, \mathbf{m} is a vector with 96 components corresponding to the counts of each of the mutation types in a sample, \mathbf{p}_i represents a vector with 96 components (corresponding to a consensus mutational signature i), e_i is a non-negative scalar reflecting the number of mutations contributed by signature i in that sample. N is equal to 12 and it reflects the number of all possible signatures that can be found in a single breast cancer sample. Mutational signatures that did not contribute large numbers (or proportions) of mutations or that did not significantly improve the correlation between the original mutational pattern of the sample and the one generated by the mutational signatures were excluded from the sample. This procedure reduced over-fitting the data and allowed only the essential mutational signatures to be present in each sample (Supplementary Table 21b).

Kataegis. Kataegis, or foci of localized hypermutation, has been previously defined²⁵ as 6 or more consecutive mutations with an average intermutation distance of less than or equal to 1,000 bp. Kataegis were sought in 560 whole-genome sequenced breast cancers from high-quality base substitution data using the method described previously²⁵. This method likely misses some foci of kataegis sacrificing sensitivity of detection for a higher positive predictive value of kataegis foci (Supplementary Table 21c).

Rearrangement signatures. *Clustered vs non-clustered rearrangements.* We sought to separate rearrangements that occurred as focal catastrophic events or focal driver amplifications from genome-wide rearrangement mutagenesis using a piecewise constant fitting method. For each sample, both breakpoints of each rearrangement were considered individually and all breakpoints were ordered by chromosomal position. The inter-rearrangement distance, defined as the number of base pairs from one rearrangement breakpoint to the one immediately preceding it in the reference genome, was calculated. Putative regions of clustered rearrangements were identified as having an average inter-rearrangement distance that was at least 10 times greater than the whole-genome average for the individual sample. Piecewise constant fitting parameters used were $\gamma = 25$ and $k_{\min} = 10$, with γ as the parameter that controls smoothness of segmentation, and k_{\min} the minimum number of breakpoints in a segment.

The respective partner breakpoint of all breakpoints involved in a clustered region are likely to have arisen at the same mechanistic instant and so were considered as being involved in the cluster even if located at a distant chromosomal site. The rearrangements within clusters ('clustered') and not within clusters ('non-clustered') are summarized in Extended Data Table 4.

Classification: types and size. In both classes of rearrangements, clustered and non-clustered, rearrangements were subclassified into deletions, inversions and tandem duplications, and then further subclassified according to size of the rearranged segment (1–10 kb, 10–100 kb, 100 kb–1 Mb, 1–10 Mb, more than 10 Mb). The final category in both groups was interchromosomal translocations.

Rearrangement signatures by NNMF. The classification produces a matrix of 32 distinct categories of structural variants across 544 breast cancer genomes. This matrix was decomposed using the previously developed approach for deciphering mutational signatures by searching for the optimal number of mutational signatures that best explains the data without over-fitting the data²⁵ (Supplementary Table 21d, e).

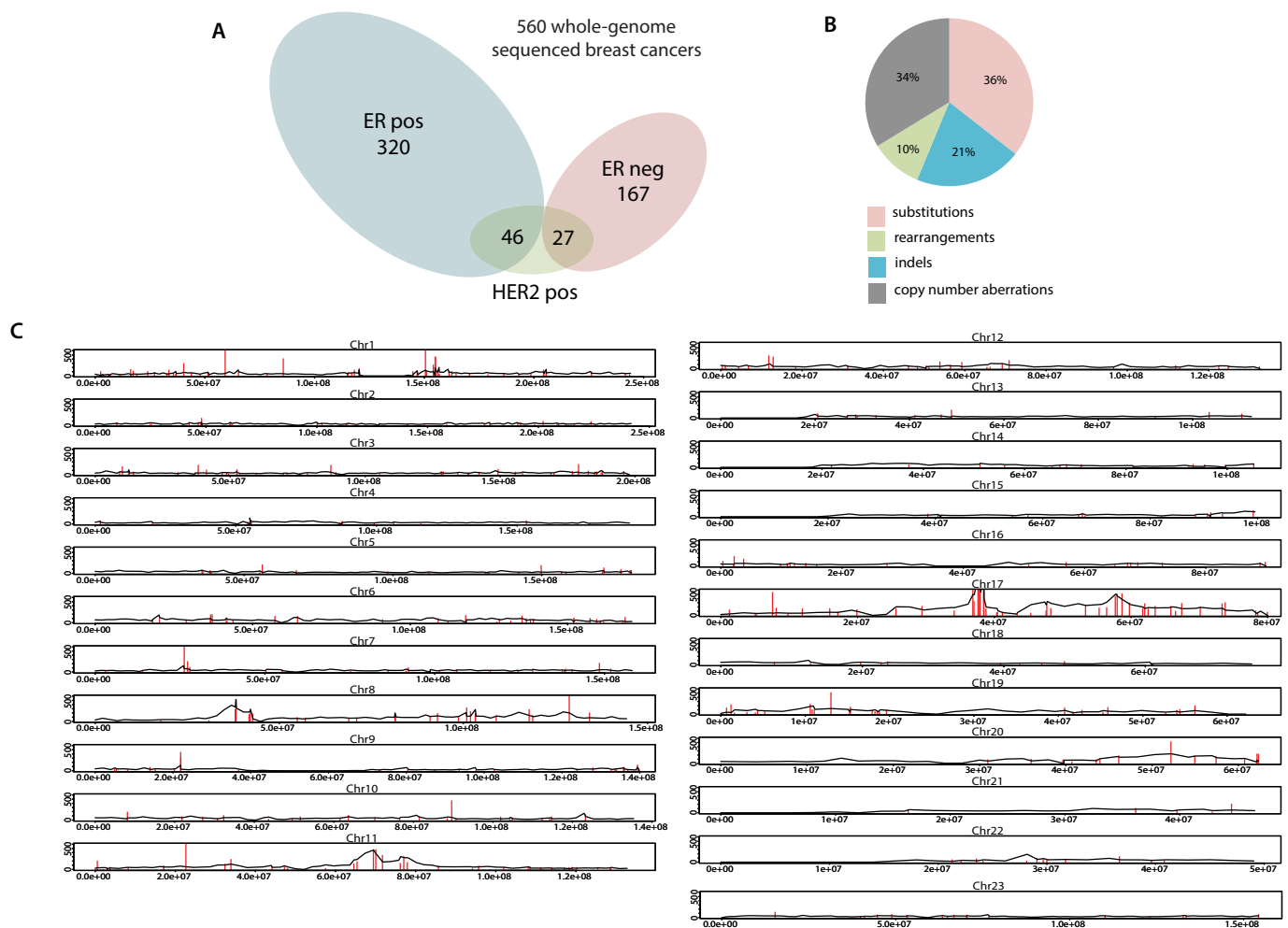
Consensus clustering of rearrangement signatures. To identify subgroups of samples sharing similar combinations of six identified rearrangement signatures derived from whole genome sequencing analysis we performed consensus clustering using the ConsensusClusterPlus R package⁵⁶. Input data for each sample ($n = 544$, a subset of the full sample cohort) was the proportion of rearrangements assigned to each of the six signatures. Thus, each sample has 6 data values, with a total sum of 1. Proportions for each signature were mean-centred across samples before clustering. The following settings were used in the consensus clustering: number of repetitions = 1000; pItem = 0.9 (resampling frequency samples); pFeature = 0.9 (resampling frequency); Pearson distance metric; Ward linkage method.

Distribution of mutational signatures relative to genomic architecture. Following extraction of mutational signatures and quantification of the exposures (or contributions) of each signature to each sample, a probability for each mutation belonging to each mutation signature (for a given class of mutation for example, substitutions) was assigned⁴².

The distribution of mutations as signatures were assessed across multiple genomic features including replication time, strands, transcriptional strands and nucleosome occupancy. See ref. 42 for technical details, per signature results.

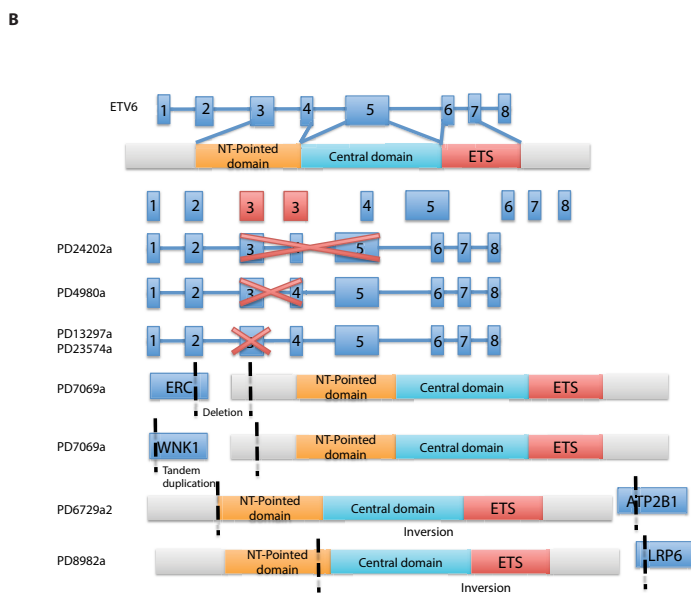
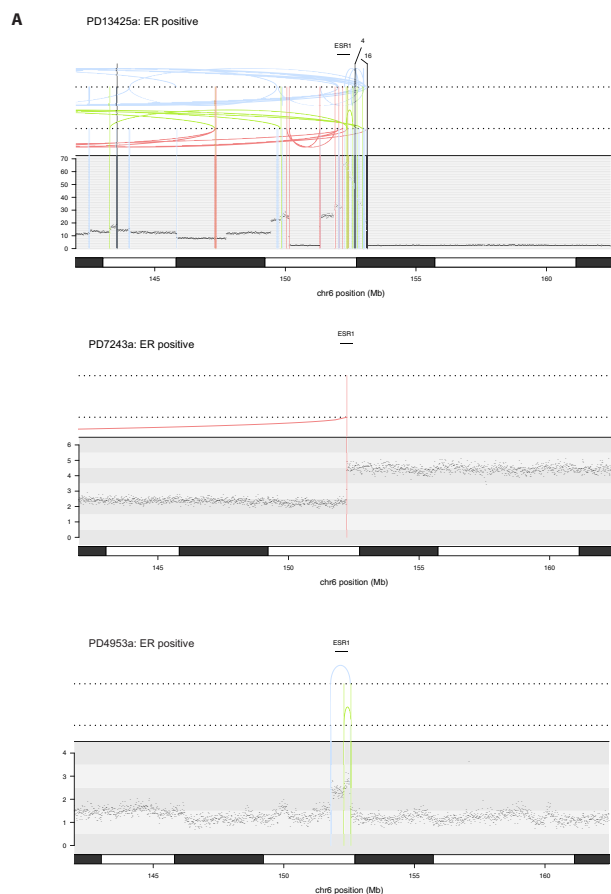
Individual patient whole-genome profiles. Breast cancer whole-genome profiles were adapted from the R Circos package⁵⁷. See <http://cancer.sanger.ac.uk/cosmic/sample/genomes> for individual patient genome profiles. Features depicted in circos plots from outermost rings heading inwards: Karyotypic ideogram outermost. Base substitutions next, plotted as rainfall plots (log₁₀ intermutation distance on radial axis, dot colours: blue, C>A; black, C>G; red, C>T; grey, T>A; green, T>C; pink, T>G). Ring with short green lines, insertions; ring with short red lines, deletions. Major copy number allele (green, gain) ring, minor copy number allele ring (pink, loss). Central lines represent rearrangements (green, tandem duplications; pink, deletions; blue, inversions; grey, interchromosomal events). In each profile, the top right-hand panel displays the number of mutations contributing to each mutation signature extracted using NNMF in individual cancers. Middle right-hand panel represents indels. Bottom right corner shows histogram of rearrangements present in this cancer. Bottom left corner shows all curated driver mutations, top- and middle-left panels show clinical and pathology data respectively.

- Kozarewa, I. *et al.* Amplification-free Illumina sequencing-library preparation facilitates improved mapping and assembly of (G+C)-biased genomes. *Nature Methods* **6**, 291–295 (2009).
- Li, H. & Durbin, R. Fast and accurate short read alignment with Burrows-Wheeler transform. *Bioinformatics* **25**, 1754–1760 (2009).
- Ye, K., Schulz, M. H., Long, Q., Apweiler, R. & Ning, Z. Pindel: a pattern growth approach to detect break points of large deletions and medium sized insertions from paired-end short reads. *Bioinformatics* **25**, 2865–2871 (2009).
- Zerbino, D. R. & Birney, E. Velvet: algorithms for de novo short read assembly using de Bruijn graphs. *Genome Res.* **18**, 821–829 (2008).
- Van Loo, P. *et al.* Allele-specific copy number analysis of tumors. *Proc. Natl Acad. Sci. USA* **107**, 16910–16915 (2010).
- Greenman, C., Wooster, R., Futreal, P. A., Stratton, M. R. & Easton, D. F. Statistical analysis of pathogenicity of somatic mutations in cancer. *Genetics* **173**, 2187–2198 (2006).
- Lawrence, M. S. *et al.* Mutational heterogeneity in cancer and the search for new cancer-associated genes. *Nature* **499**, 214–218 (2013).
- Sun, L., Craiu, R. V., Paterson, A. D. & Bull, S. B. Stratified false discovery control for large-scale hypothesis testing with application to genome-wide association studies. *Genet. Epidemiol.* **30**, 519–530 (2006).
- The ENCODE Project Consortium An integrated encyclopedia of DNA elements in the human genome. *Nature* **489**, 57–74 (2012).
- Wilkerson, M. D. & Hayes, D. N. ConsensusClusterPlus: a class discovery tool with confidence assessments and item tracking. *Bioinformatics* **26**, 1572–1573 (2010).
- Zhang, H., Meltzer, P. & Davis, S. RCircos: an R package for Circos 2D track plots. *BMC Bioinformatics* **14**, 244 (2013).



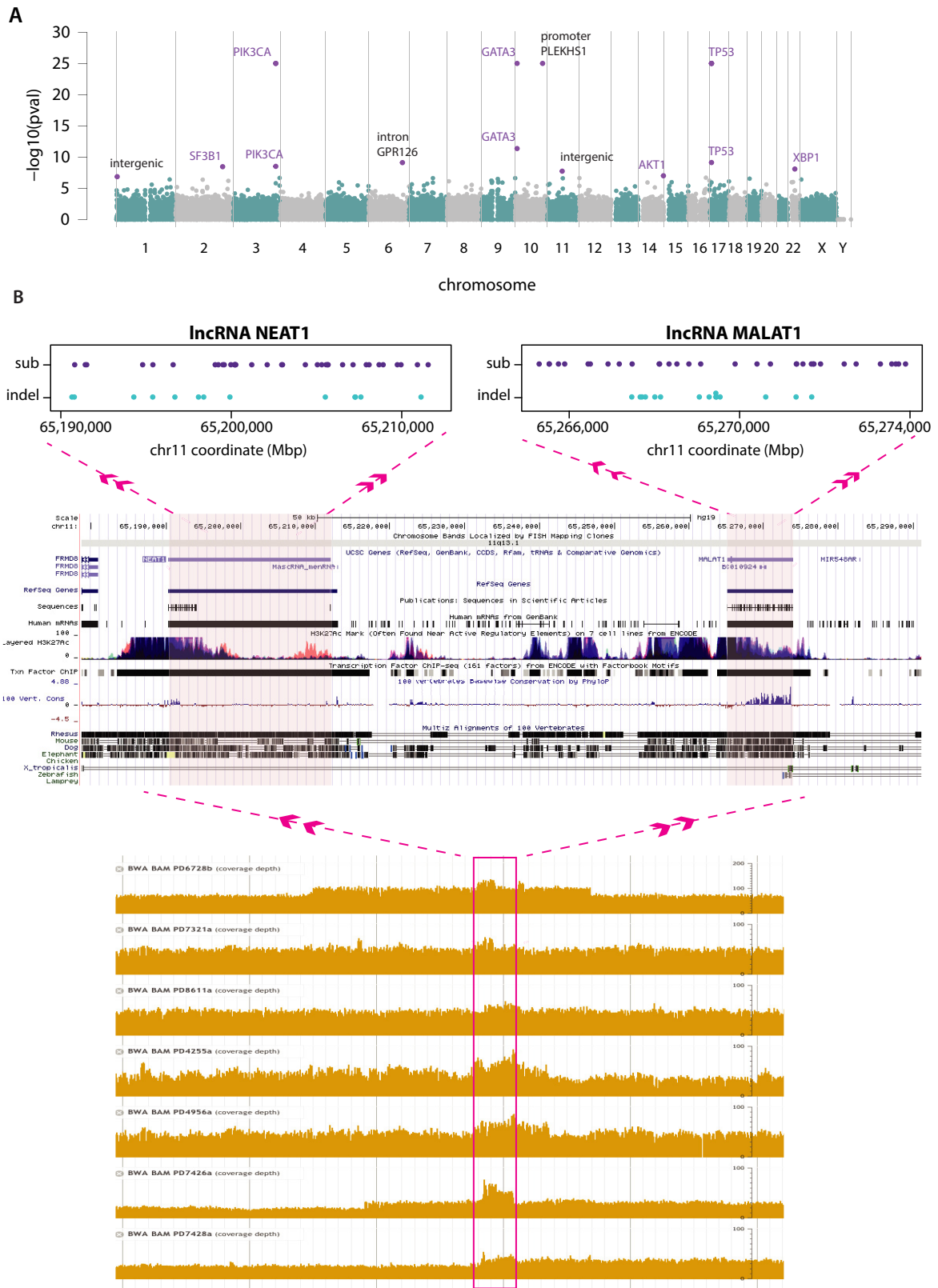
Extended Data Figure 1 | Landscape of driver mutations. **a**, Summary of subtypes of cohort of 560 breast cancers. **b**, Driver mutations by mutation type. **c**, Distribution of rearrangements throughout the genome. Black

line represents background rearrangement density (calculation based on rearrangement breakpoints in intergenic regions only). Red lines represent frequency of rearrangement within breast cancer genes.



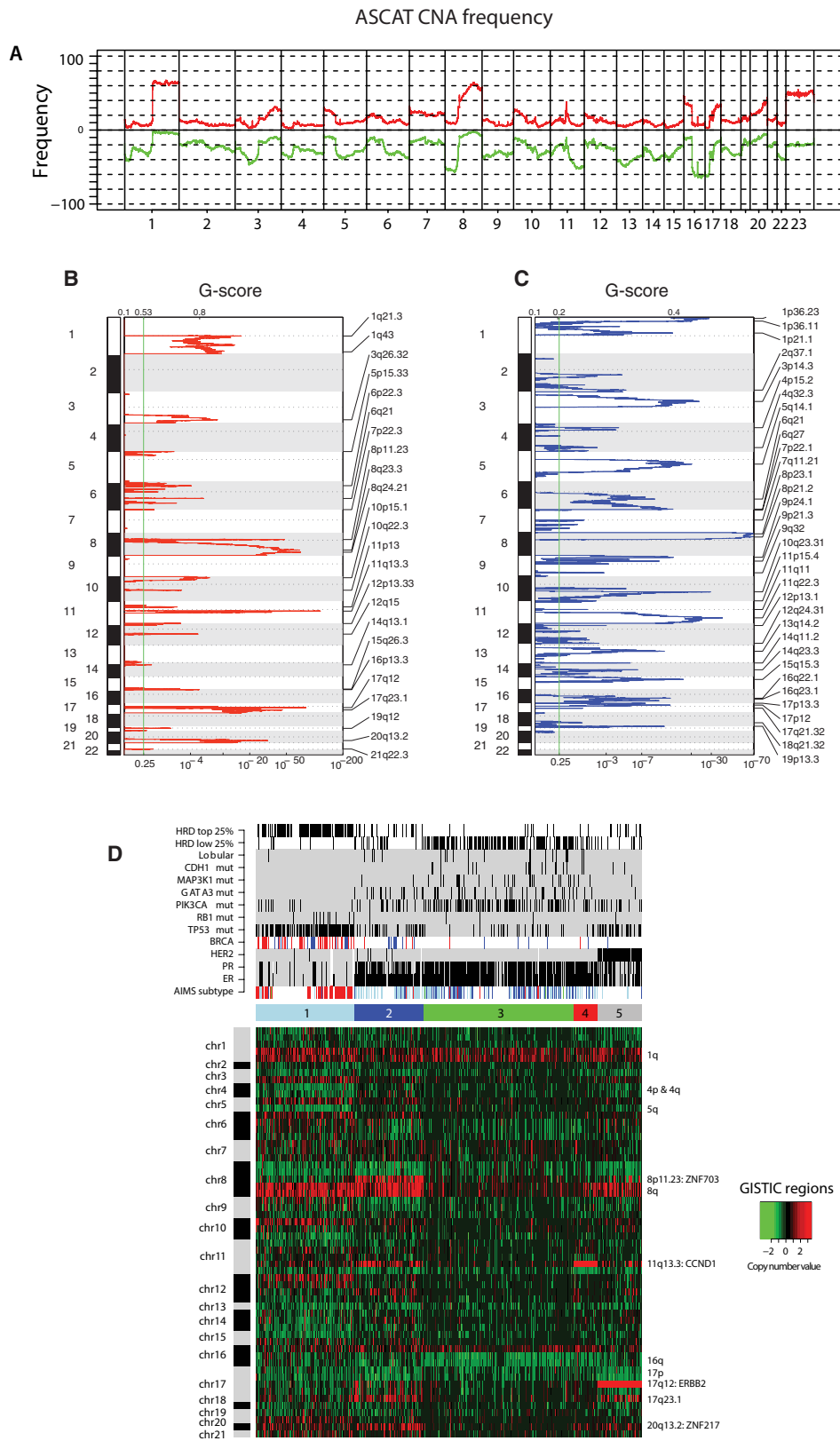
Extended Data Figure 2 | Rearrangements in oncogenes. a, Variation in rearrangement and copy number events affecting *ESR1*. Clear amplification in top panel, translocation of *ESR1* in middle panel and focused tandem duplication events in bottom panel. **b**, Predicted outcomes of some rearrangements affecting *ETV6*. Red crosses indicate exons

deleted as a result of rearrangements within the *ETV6* genes, black dotted lines indicate rearrangement break points resulting in fusions between *ETV6* and *ERC*, *WNK1*, *ATP2B1* or *LRP6*. *ETV6* domains indicated are: N-terminal (NT) pointed domain and E26 transformation-specific DNA binding domain (ETS).



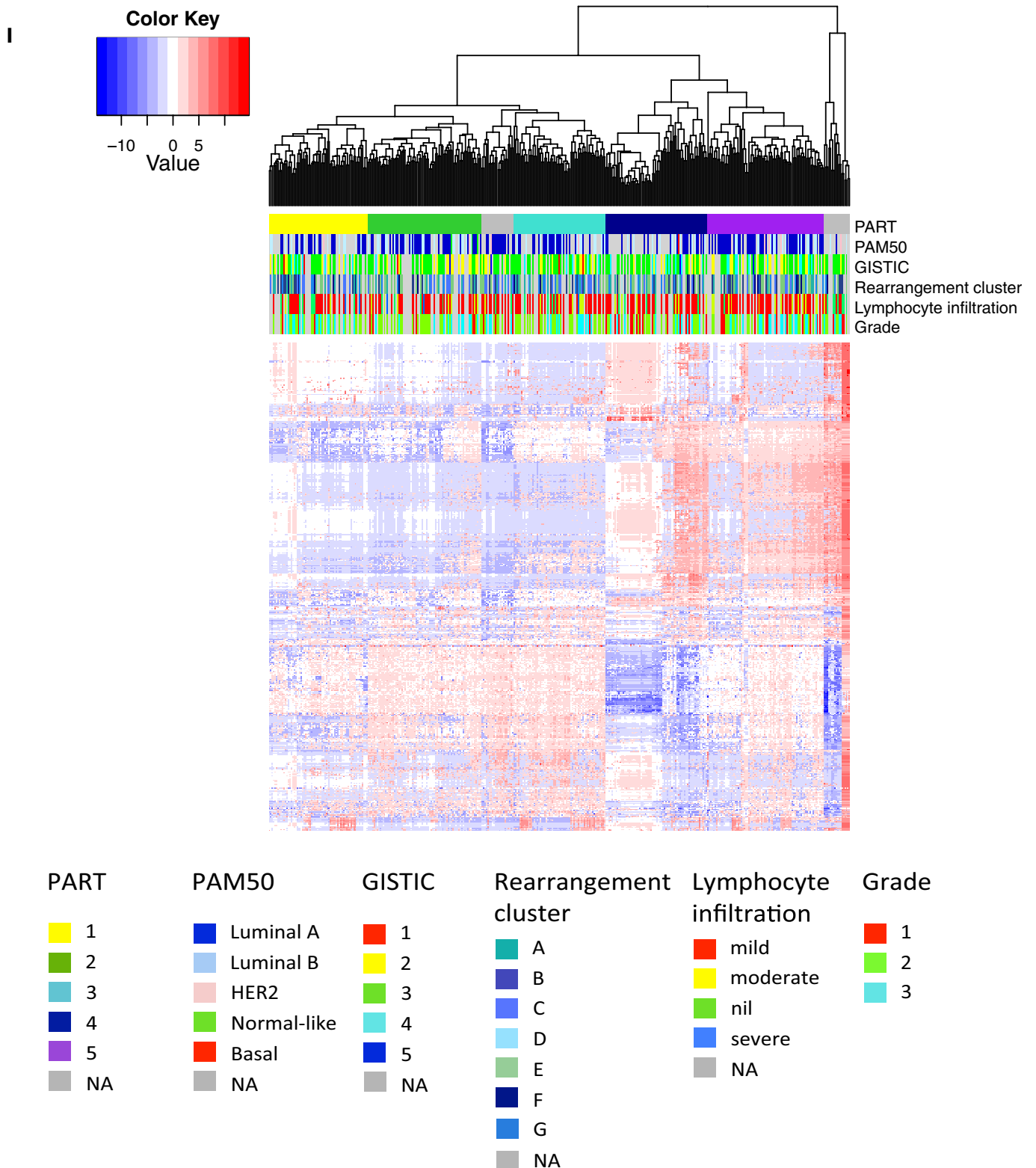
Extended Data Figure 3 | Recurrent non-coding events in breast cancers. **a**, Manhattan plot demonstrating sites with most significant P values as identified by binning analysis. Purple highlighted sites were also detected by the method seeking recurrence when partitioned by genomic features. **b**, Locus at chr11 65 Mb, which was identified by independent analyses as being more mutated than expected by chance.

Bottom, a rearrangement hotspot analysis identified this region as a tandem duplication hotspot, with nested tandem duplications noted at this site. Partitioning the genome into different regulatory elements, an analysis of substitutions and indels identified lncRNAs *MALAT1* and *NEAT1* (topmost panels) with significant P values.



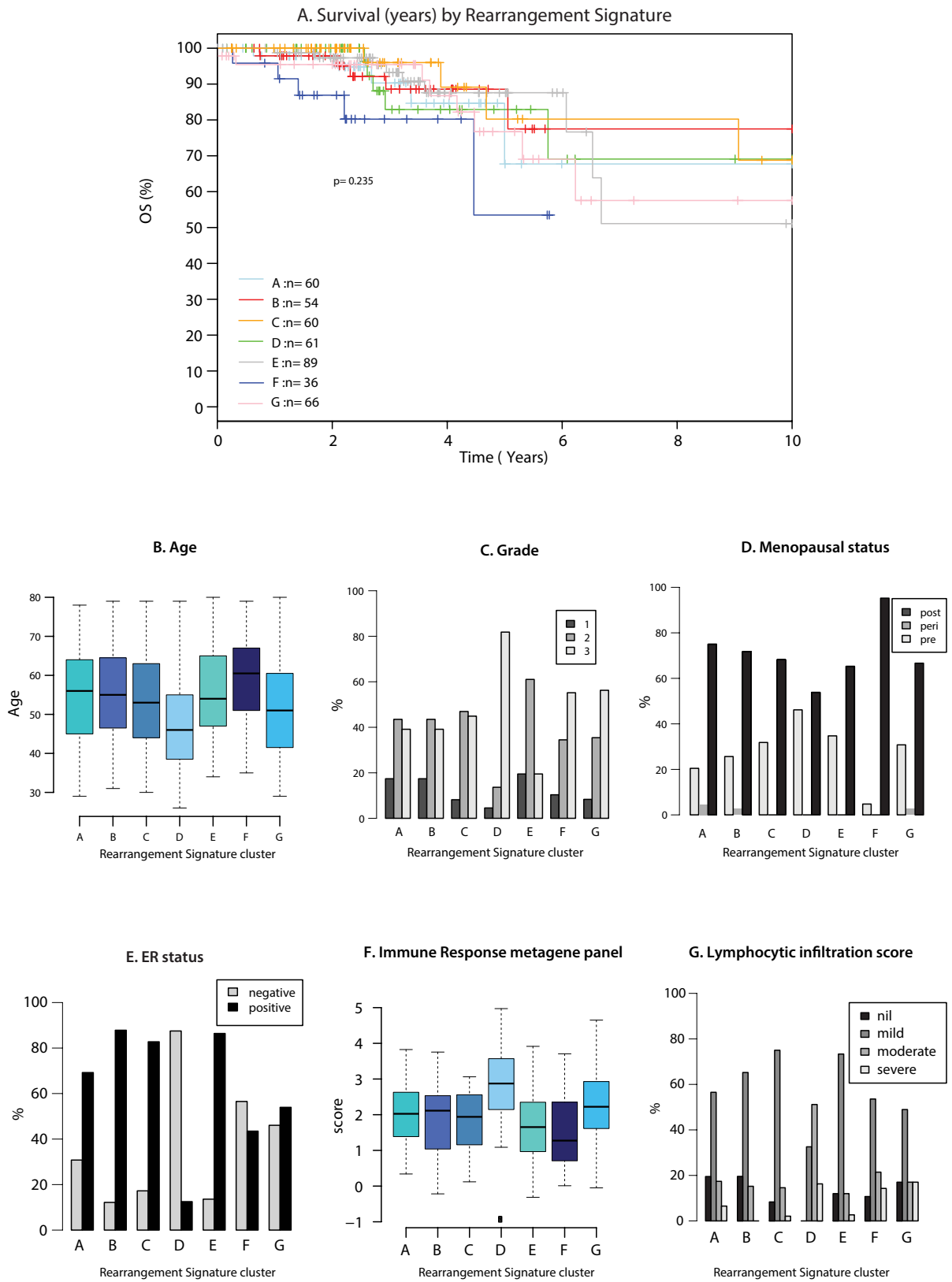
Extended Data Figure 4 | Copy number analyses. **a**, Frequency of copy number aberrations across the cohort. Chromosome position along *x* axis, frequency of copy number gains (red) and losses (green) *y* axis. **b**, Identification of focal recurrent copy number gains by the GISTIC method (Supplementary Methods). **c**, Identification of focal recurrent copy number losses by the GISTIC method. **d**, Heatmap of GISTIC regions following unsupervised hierarchical clustering. Five cluster

groups are noted and relationships with expression subtype (basal, red; luminal B, light blue; luminal A, dark blue), immunohistochemistry status (ER, PR, HER2 status; black, positive), abrogation of *BRCA1* (red) and *BRCA2* (blue) (whether germline, somatic or through promoter hypermethylation), driver mutations (black, positive), HRD index (top 25% or lowest 25%; black, positive).



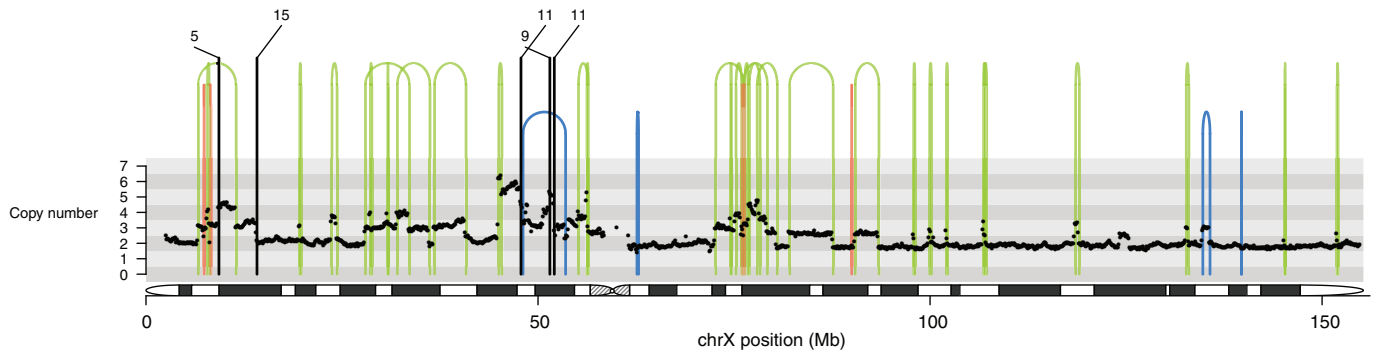
Extended Data Figure 5 | miRNA analyses. Hierarchical clustering of the most variant miRNAs using complete linkage and Euclidean distance. miRNA clusters were assigned using the partitioning algorithm using recursive thresholding (PART) method. Five main patient clusters were revealed. The horizontal annotation bars show (from top to bottom):

PART cluster group, PAM50 mRNA expression subtype, GISTIC cluster, rearrangement cluster, lymphocyte infiltration score and histological grade. The heatmap shows clustered and centred miRNA expression data (\log_2 transformed). Details on colour coding of the annotation bars are presented below the heatmap.

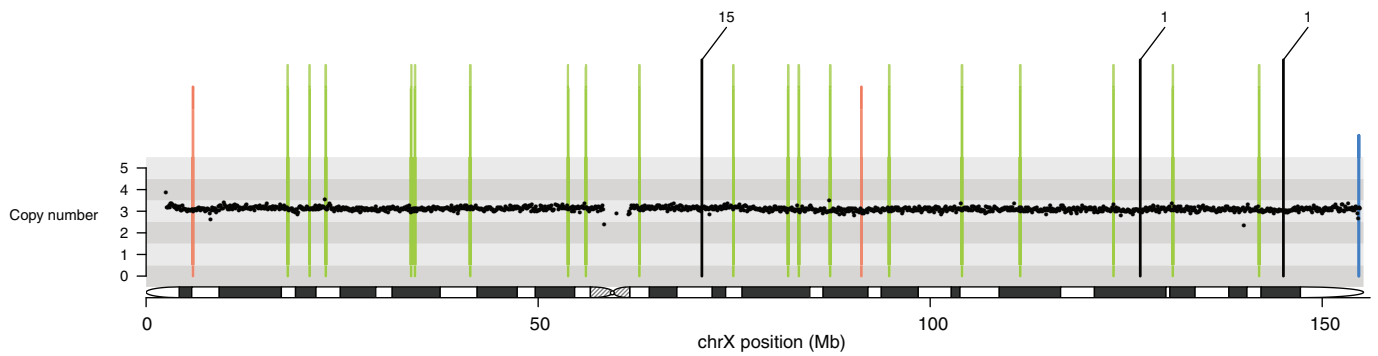


Extended Data Figure 6 | Rearrangement cluster groups and associated features. a, Overall survival (OS) by rearrangement cluster group. b, Age of diagnosis. c, Tumour grade. d, Menopausal status. e, ER status. f, Immune response metagene panel. g, Lymphocytic infiltration score.

PD4841a chromosome X

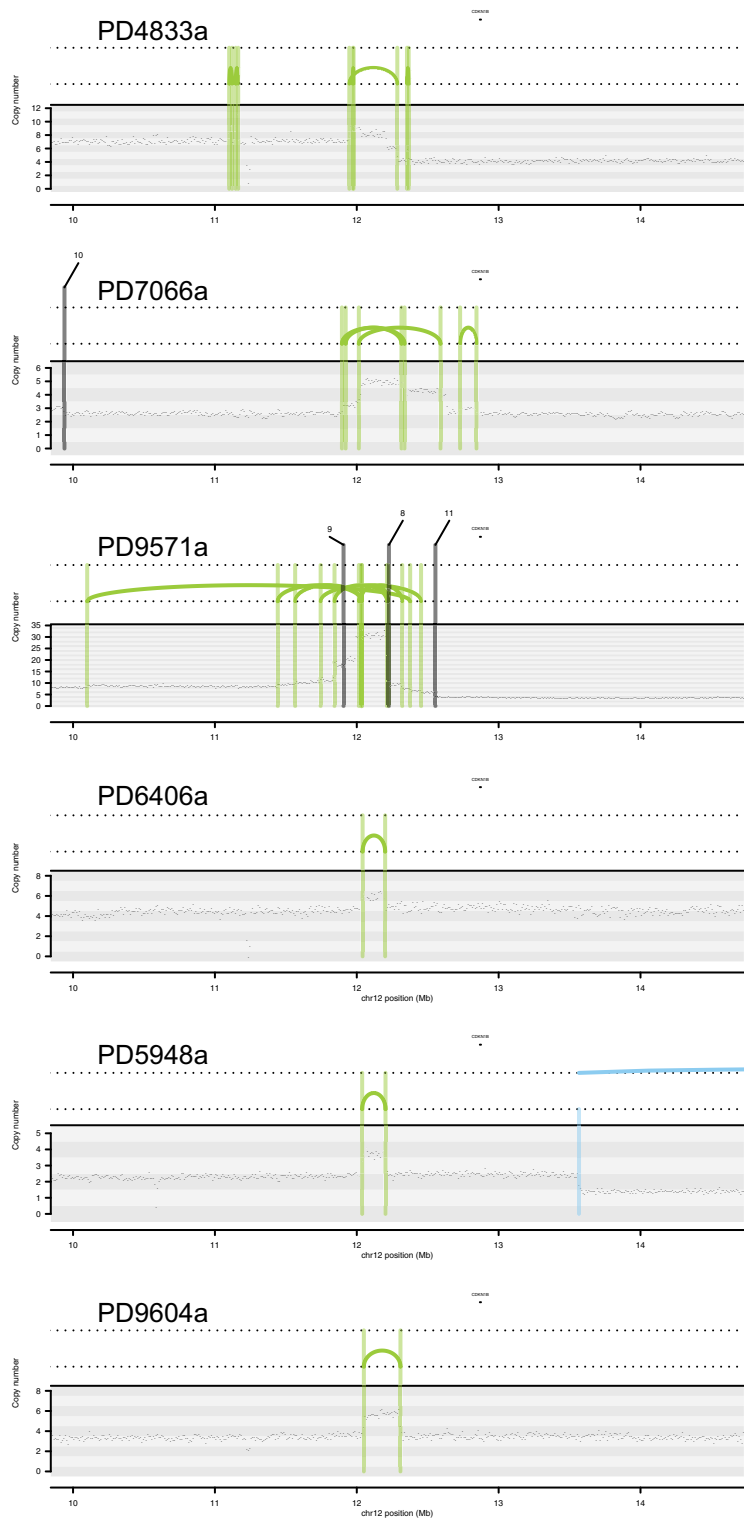


PD4833a chromosome X

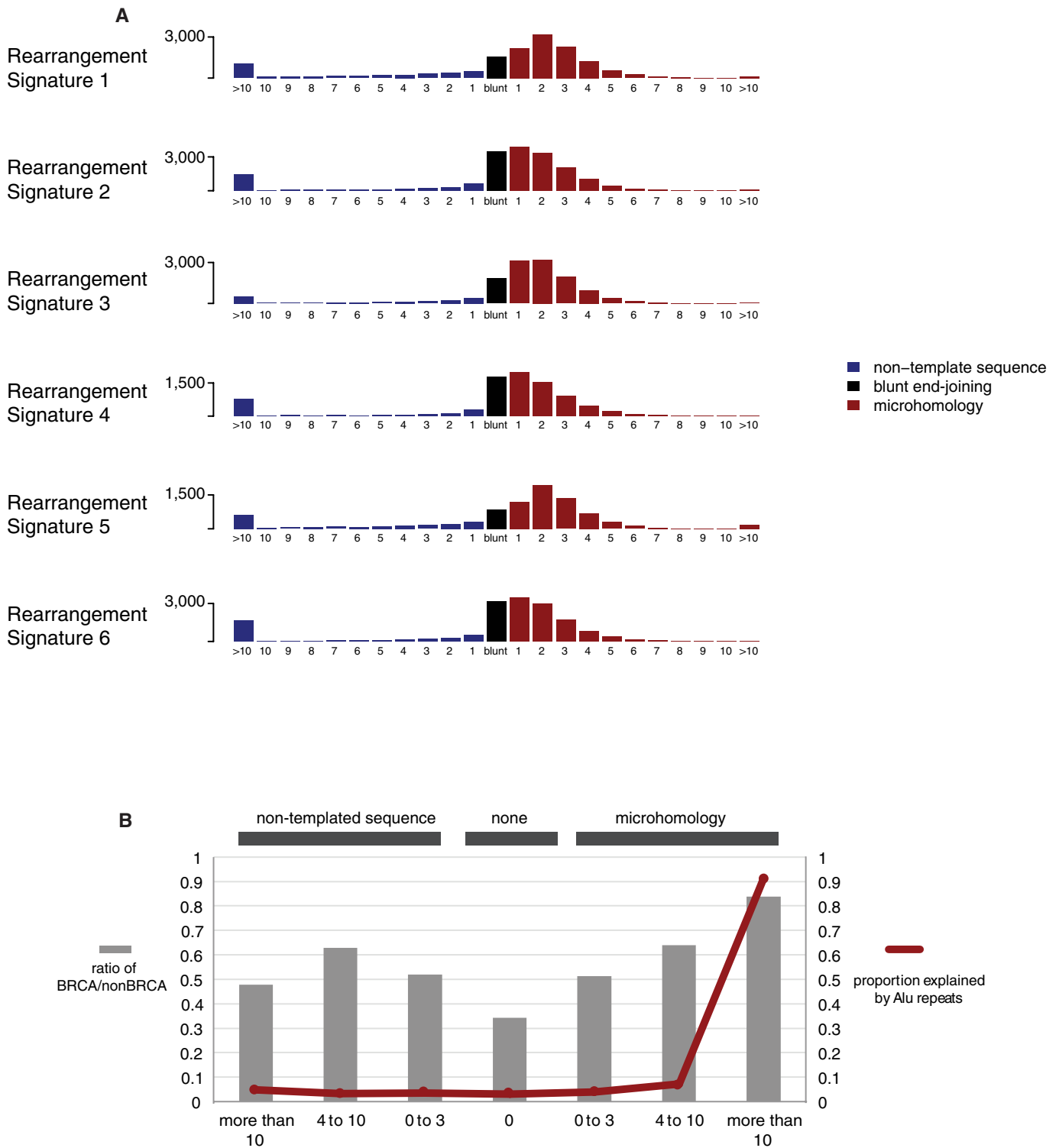


Extended Data Figure 7 | Contrasting tandem duplication phenotypes. Contrasting tandem duplication phenotypes of two breast cancers using chromosome X. Copy number (*y* axis) depicted as black dots. Lines represent rearrangements breakpoints (green, tandem duplications; pink, deletions; blue, inversions; black, translocations with partner

breakpoint provided). Top, PD4841a has numerous large tandem duplications (>100 kb, rearrangement signature 1), whereas PD4833a has many short tandem duplications (<10 kb, rearrangement signature 3) appearing as 'single' lines in its plot.

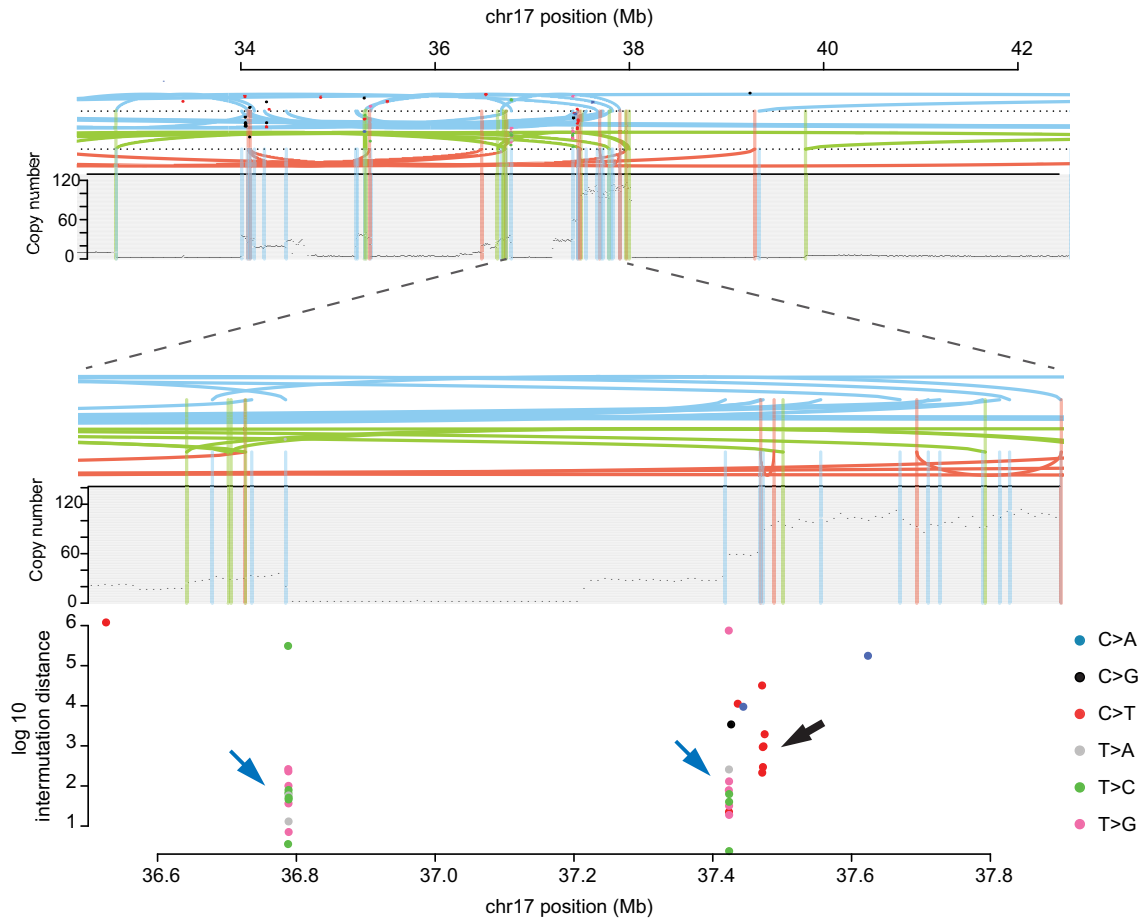


Extended Data Figure 8 | Hotspots of tandem duplications. A tandem duplication hotspot occurring in six different patients.

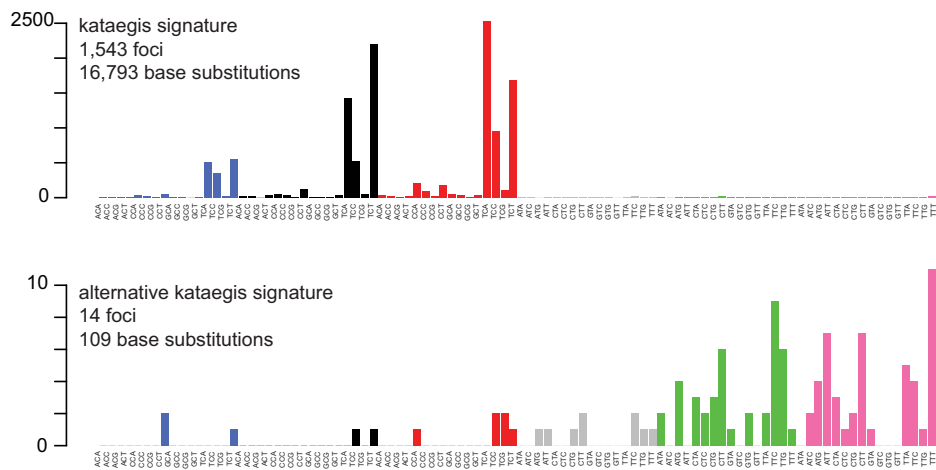


Extended Data Figure 9 | Rearrangement breakpoint junctions. a, Breakpoint features of rearrangements in 560 breast cancers by rearrangement signature. b, Breakpoint features in BRCA and non-BRCA cancers.

A



B



Extended Data Figure 10 | Signatures of focal hypermutation.

a, Kataegis and alternative kataegis occurring at the same locus (ERBB2 amplicon in PD13164a). Copy number (y axis) depicted as black dots. Lines represent rearrangements breakpoints (green, tandem duplications; pink, deletions; blue, inversions). Top, an ~10 Mb region including the ERBB2 locus. Middle, zoomed-in tenfold to an ~1 Mb window

highlighting co-occurrence of rearrangement breakpoints, with copy number changes and three different kataegis loci. Bottom, demonstrates kataegis loci in more detail. \log_{10} intermutation distance on y axis. Black arrow, kataegis; blue arrows, alternative kataegis. **b**, Sequence context of kataegis and alternative kataegis identified in this data set.